NATIONAL ADVISORY COMMITTEE FOR AERONAUTICS

TECHNICAL MEMORANDUM 1397

INTERIM REPORT ON FATIGUE CHARACTERISTICS OF A TYPICAL METAL WING

By J. L. Kepert and A. O. Payne

Aeronautical Research Laboratories
Melbourne, Australia

Washington
March 1956

CONTENTS

NATIONAL ADVISORY COMMITTEE FOR AERONAUTICS

TECHNICAL MEMORANDUM 1397

INTERIM REPORT ON FATIGUE CHARACTERISTICS OF A TYPICAL METAL WING[1]

By J. L. Kepert and A. O. Payne

SUMMARY

The results of fatigue tests on seventy-two P51D "Mustang" mainplanes are reported. The object of the programme is to investigate the fatigue characteristics of a riveted wing structure under all practical combinations of alternating load and mean load.

Tests were made on a number of specimens at each of a series of load ranges and on many of these specimens the stress distribution was determined during the test by electric resistance strain gauges. A series of tests was also done on specimens subjected to pre-loads of up to 95 percent of the ultimate failing load. Tests at relatively high load ranges were done in an hydraulic loading rig while the tests at lower loads with consequent longer life were done in a more rapid resonant vibration rig.

From the test data at present available the following conclusions may be drawn:

(a) The frequency of occurrence of any one type of failure appears to be related to the load range.

(b) The rate of propagation of visible cracks is approximately constant for a large part of the life.

(c) The fatigue strength of the structure is similar to that of the notched material for an appropriate theoretical stress concentration factor which is greater than 3.0.

(d) The frequency distribution of fatigue life is approximately logarithmic normal.

---

[1] This paper, reproduced by NACA through the courtesy of the Department of Supply, Commonwealth of Australia, was originally published as Report ARL/SM. 207, Melbourne, Australia, January 1955.

(e) The relative increase in fatigue life for a given pre-load is a function of the maximum load of the loading cycle only. The optimum value of pre-load for this structure is approximately 85 percent of the ultimate failing load.

(f) In determining the fatigue strength of a critical component in a redundant structure, the local stress level cannot be obtained with sufficient accuracy using the normal design procedure.

1. INTRODUCTION

The present programme of tests on Mustang wings was undertaken as a continuation of the investigation on the fatigue strength of metal wing structures begun on "Boomerang" CA-12 wings in 1948.

The aims of the programme are:

(a) To observe the behaviour of a typical wing structure subjected to repeated loading and, following the earlier works, to obtain information on some aspects of fatigue failure including, the dependence of the type of failure on the load range, the rate of crack propagation and the nature of the stress distribution in the critical areas.

(b) To determine the complete alternating load-mean load diagram for a full scale wing of typical riveted construction.

(c) To correlate the fatigue strength of a complete structure to notched fatigue data on the component material.

(d) To examine the form of the frequency distribution of fatigue life and obtain the fatigue life for given probability levels.

(e) To investigate the effect of pre-loading on the fatigue characteristics of the structure.

Ninety-one "Mustang" wings, declared surplus following World War II were procured for this programme and in pursuance of the above objectives these specimens are tested to destruction without modification. Initial results have already been reported in reference 1 but all results on the seventy-two wings tested up to the present date are included here.

2. DESCRIPTION OF TEST SPECIMENS

The wing is of stressed skin construction, fabricated mainly from 24 ST alclad sheet and 24 ST extruded sections. It consists of two

tapered panels having a main and rear spar. (See figs. 2, 3, and 5.) Outboard of station 145 the torsion box is formed by the upper and lower surfaces and the rear spar. Between stations 145 and 75 the torsion box is formed by the leading edge and main spar and between stations 75 and 0 by the wing surfaces and the front and rear spars. The two wing panels are joined at the centre by internal bolting angles on the upper surface and external bolting angles on the lower surface. This structure is regarded as a typical example of the sheet and stringer construction being used in aircraft structures at the present time.

While none of the wings tested was virgin, only nine had seen much service. The remainder had experienced very little flying and this consisted mostly of acceptance tests and ferrying flights. The average flying time of these specimens was 65 hours, varying from 13 to 365 hours. The remaining nine wings had seen operational service in Korea and each had experienced over 500 hours flying. (Their flying time is noted in table I.) As mentioned in section 8 it is proposed to investigate the effect of previous flying time on the fatigue life.

3. METHOD OF TESTING

3.1 Loading Condition

The test loads represented the low angle of attack case and were derived from reference 2. The shear and torsion diagrams are shown in figure 1.

The ultimate load factor used in design was 12 for an aircraft weight of 8,000 lb. However the test loads are expressed as a percentage of the ultimate failing load (U.F.L. = 89,600 lb) which was determined as reported in reference 3.

3.2 Hydraulic Loading Method

The tests at high load and relatively short life (less than about 30,000 cycles) were done in an hydraulic loading rig (ref. 4). In tests where the mean load was relatively low the minimum load of the cycle was a download. For these tests weights were stacked upon the upper surface of the wing and distributed in such a manner that the required bending moment and shear force distribution were obtained.

When using this method screw jacks were used to tension the holding down straps and support the dead weight load as shown in figure 7. At the normal rate of cycling of 10 c.p.m the weights showed no slip during the test. A specimen loaded with weights for testing in this manner is shown in figure 6.

3.3 Vibration Loading Method

The tests at low load range were done in a vibration loading rig, a general view of which is shown in figures 8 and 9. This method was a development of that originally used in the fatigue testing of CA-12 wings (ref. 15). Fixed suspension was used thus obtaining the correct loading throughout the span. This proved an essential requirement as major failures were obtained in the neighbourhood of the fuselage connections. The method of testing consisted of modifying the structure by attaching masses, or springs of suitable stiffness, so that when the structure was vibrated at its natural frequency the required shear load distribution was applied. The vibration was excited on the port side by a stroking machine driving through a spring, the load being controlled by a deflection indicator at the starboard tip.

A detailed description of the test rig together with the method of calculating the vibration mode is given in appendices I and II. The accuracy of loading has been checked by numerous electric resistance strain gauge readings and also by deflections measured during the test. From this investigation which is described in appendix II it appears that the applied load is accurately known to within ±5 percent. To improve on this estimate more accurate methods of measuring the relatively small strains and deflections would have to be developed.

The test data shows that at these low load ranges a variation of ±5 percent in the alternating load results in a variation of approx. ±25 percent in the mean life. This is relatively small compared to the total variation in life about the mean value which at these load ranges gives a value of about $6\frac{1}{2}$:1 for the ratio of the lives to failure at probability levels of 0.99 and 0.01.

4. DESCRIPTION OF TESTS

Tests in the hydraulic loading rig were continued until final failure occurred and in the vibration loading rig until it was observed to be imminent.

No modifications or repairs were made to the structure either before or during testing but bolts and screws that failed during a test were replaced wherever possible.

For each specimen the life of both port and starboard halves has to be determined either by testing the unbroken half with a mating half from another wing (a composite specimen) or by estimating the remaining life

from the results of other similar tests. All loads have been expressed as percentages of the ultimate failing load as determined in reference 3.

4.1 The Alternating Load - Mean Load Diagram

To determine the alternating load - mean load diagram tests at a series of different alternating loads were carried out at mean loads of 6 percent, 27 percent, 37 percent, 47 percent, and 68 percent. The tests at 6 percent mean load were done in the Vibration Loading Rig except for the high alternating load tests at 3 ± 35 percent U.F.L. The Hydraulic Rig was used for all the other tests.

4.2 The Effect of Pre-Load

The effect of a pre-load on the fatigue life has been investigated by varying the following parameters:

(a) Magnitude of the pre-load. Specimens were subjected to pre-loads of 70 percent, 85 percent, 90 percent, and 95 percent U.F.L. In each case the effect of the pre-load on the fatigue life was then determined by testing two wings at a given load range namely 6 ± 28 percent.

(b) Values of the load range. The effect on the fatigue life of a given pre-load (95 percent U.F.L.) has been determined for different alternating loads namely 11 percent and 28 percent at a constant mean load of 6 percent.

Similarly, the effect at different mean loads has been determined by testing specimens pre-loaded to 85 percent at mean loads of 6 percent and 37 percent and constant alternating load of 28 percent.

Two specimens pre-loaded to 85 percent have been tested at an intermediate load range of 27 ± 16 percent. Details of these tests are shown in table II.

4.3 Investigation of the Strain Distribution

Electric resistance strain gauges were attached to a number of specimens in areas which experience has shown contained the major failures, in order to determine the local stress and the manner in which it varied as failure progressed. The strain readings were taken on a Miller Oscillograph for wings tested in the Vibration Rig and on a Tinsley Recorder for tests in the Hydraulic Rig.

Also the wings tested in the Vibration Rig were first loaded in the Hydraulic Rig and the strain gauges calibrated in terms of load using the Miller Oscillograph so that a direct comparison between the loads applied in the two test rigs was obtained. Tests are in progress to determine the strain distribution in critical areas before and after pre-loading, by applying pre-loads of successively increasing magnitude.

5. TEST RESULTS

The port and starboard sides of the wing are structurally identical except for minor differences which did not affect the fatigue failures, and each half wing has therefore been regarded as a test specimen. This gives double the number of test results but it is essential to determine a life for each half so that the strongest are not excluded.

For specimens tested up to the present time the average life of port mainplanes is 13 percent greater than that of starboard. Although a preliminary examination indicates that there is statistical significance at the 5 percent level the difference is regarded as negligible for practical purposes.

A summary of the test data for all specimens is shown in table I. The alternating load-mean load diagram (A-M diagram) of figure 24 has been obtained from S-N curves plotted for a series of mean loads between 0 and 70 percent U.F.L. The cycles to failure at each load range has been taken to be the mean life, determined on a logarithmic basis, for the specimens tested. This method is used because, as is shown later (appendix IV), the distribution of the log of the life in the neighbourhood of the mean is a very good approximation to the normal distribution. The tests, particularly at 16 percent mean load, are not yet complete and the shapes of the constant life lines in figure 24 are therefore not final.

Six distinct types of failure have been observed at positions indicated in figure 5. These can be summarised as:

I. Failure initiating in the skin at station 80 from the leading edge of the ammunition chute.

II. Failure in the region of station 21, originating from the junction of the wheel-well panel with the front spar.

III. Failure in the region of station 28 originating from the front spar flange where the spar doubler ends.

IV. Failure in the region of station 6 originating from holes required for the bolts attaching the joint cap at the centre joint.

V. Failure initiating similarly to III in the region of station 35.

VI. In pre-loaded wings only; failure in the upper flange of the front spar at station 77, leading to failure in the lower flange and then forward into the skin from the front outboard corner of the tank-bay. The failures are described in detail in appendix III.

The results on the effect of pre-loading are shown in table II. Graphs of the relative increase in fatigue life as a function of the magnitude of the pre-load and as a function of the maximum load of the loading cycle are shown in figures 27 and 28 respectively. The points plotted represent the results of pre-load tests on two wings in each case, except for the 85 percent pre-load at a test load of 6 ± 11 percent where only one starboard specimen was tested.

The strain distribution in the critical area of the tank-bay is shown in figure 33. These readings were taken in the region of the front spar between stations 15 and 40 where the failures II, III, and V develop.

6. DISCUSSION OF RESULTS

Referring to the A-M diagram of figure 24, the lines of constant life are of similar shape to those for notched specimens of 24 ST aluminium alloy derived from references 6 and 7. Unfortunately very little data are available on notched 24 ST alclad which is the main material used in the tension surface. However in Appendix V a comparison has been made between the fatigue strength of the Mustang specimens and that of the clad material for load range ratio $R = 0$. This comparison indicates that although the location of the failure varies with the load range, the life to final failure always corresponds to a value of the theoretical stress concentration factor $\left(K_T\right)$ of approximately 3.6.

In appendix VI it is shown that the fatigue life of a large riveted structure, when compared with that of the notched material at the same nominal stress, would be expected to show a value of K_T greater than 3.0. The results on Mustang specimens, for $R = 0$ at least, support this conclusion for independent failures in quite different areas. If a value of K_T greater than 3.0 always applies for the life to complete collapse, as suggested, the fatigue strength of this type of construction will always be limited considerably by that of the component material.

The statistical distribution of fatigue life has been investigated in appendix IV. At each point on the A-M diagram the logarithms of the lives have been taken and standardised to correspond to a population with zero mean and unit standard deviation, the resulting cumulative distribution being shown in figure 32. In the neighbourhood of the mean

value the results show good agreement with the straight line representing the normal variable although extreme values diverge from it. In appendix IV it is shown that the method used by A. M. Freudenthal (ref. 5) to explain this behaviour on theoretical grounds for plain material specimens may also be applied to final failure in the Mustang wings. This together with the fact that the results include failures in quite different areas of the wing, indicates that the logarithmic normal should be a good approximation to the distribution of fatigue life for riveted structures in general.

Using the cumulative frequency distribution plotted in figure 32 constant life lines for probabilities of failure P, of 0.01 and 0.99, have been drawn on the A–M diagram in figure 25. These data are best applied to an individual case by drawing S–N curves for the appropriate mean load for probabilities of failure of 0.01 and 0.99, using figure 25. This has been done for mean loads of 0 percent, 15 percent, 30 percent, and 45 percent as shown in figure 26.

The ratio of the lives corresponding to probabilities of failure of 0.99 and 0.01 varies with the load range but the average value is approximately 2.5:1.

It should be noted that these diagrams of life to failure refer to a half mainplane and at the same probability level do not give the life for a P51D wing which would have a lower value since failure of either half constitutes failure of the complete specimen. As the port and starboard halves are considered identical this can be regarded purely as a size effect and the theory due to Weibull applied (ref. 10). On that basis if P_2 is the probability of failure of the complete wing and P_1 that of either port or starboard half:

$$P_2 = 1 - (1 - P_1)^2$$

Data can therefore be obtained for a complete wing at a probability level P_2 by using a value of $P_1 = 1 - \sqrt{1 - P_2}$. Thus for the life lines of figure 24, $P_1 = 0.5$, and these are hence life lines of $P_2 = 0.75$ for the complete wing. To obtain the mean life lines ($P_2 = 0.5$), lines corresponding to a value of $P_1 = 1 - \frac{1}{\sqrt{2}}$ would be taken from the data.

A statistical analysis of the results given in appendix IV shows that the type of failure is not influenced by the magnitude of the alternating load of the cycle. At the present time the data indicates that the mean load and the maximum load both have a significant effect on the type of failure, but it is hoped to clarify this when the tests are completed.

There is an optimum value of pre-load giving a maximum relative increase in fatigue life, as shown in figure 27, for the load range of 6 ± 28 percent. At this load range the optimum value of pre-load is 83 percent. Heavily pre-loaded specimens tested at low mean loads have developed major fatigue failures in the upper surface as shown in the long life tests at 6 ± 10.6 percent where all the pre-loaded specimens showed fatigue cracks passing through the upper flanges of both front and rear spars from the corners of the gunbay opening (the first stage of failure type VI). This is caused by the unfavourable stress redistribution induced in the upper surface, (normally in compression) which in low mean load tests is subjected to relatively high alternating tension.

Referring to figure 28 the relative increase in fatigue life for a given pre-load, when plotted against the maximum load of the cycle gives a smooth curve. This applies for both pre-load values of 85 percent and 95 percent for each of which tests have been done at three different load ranges. No such relationship is found between the relative increase in life and the other parameters of the load range, which indicates that the relative increase in life at a given pre-load is a function of the maximum load of the loading cycle only. These curves have been used therefore to show the behaviour of the pre-loaded structure at all load ranges and are referred to simply as the pre-load curves. Since the beneficial effect of pre-loading approaches zero as the maximum load of the cycle approaches the pre-load, the pre-load curves have been drawn tangent to the axis of load at a point corresponding to the pre-load for which they apply. The shape of the curves then shows that the optimum value of pre-load is practically the same for all load ranges. Also as the maximum load of the cycle is decreased the relative increase in fatigue life increases steadily and, for pre-loads near the optimum, becomes very great. This results in the fatigue failure being transferred to the upper surface (the surface in compression under the pre-load) as already explained. To further investigate these effects tests are in progress to determine the local stress distribution and force redistribution that occurs in the critical members as the magnitude of the pre-load is increased.

The strain distribution along the front spar between station 15 and station 42 is shown in figure 33. These results have been obtained from electric resistance strain gauges attached to the main spar flange, the tank-bay door, and the skin panel attached to the front spar flange rear of the wheel well. This is the region in which failure types II, III, and V originate.

Peak stresses[2] occur in the spar flange at station 28 where the spar doubler ends and near station 21 where the wheel well panel ends. Corresponding peak stresses occur in the tank-bay door. The heavy doubling plate on the wheel well skin panel ends at station 37 and between this

[2]NACA reviewer observes that these peak stresses would correspond with the strains of figure 33.

point and station 20, the stress carried in the skin panel falls off considerably causing a corresponding rise in the stress in the main spar flange. These results show that the major fatigue failures occur at points where there is a peak in the local stress level.

The design stress, based on simple engineering bending theory, is shown in figure 33 for comparison. The stresses in the three members, main spar flange, tank-bay door and skin panel are all equal and local stress variation is simply proportional to the local change in section modulus. It is apparent that the errors in the actual local stress distribution are so marked that the normal design stress cannot be used successfully in the determination of the fatigue strength of the structure.

The rates of crack propagation at the major failures are shown in figure 14 and 15 from which it will be observed as noted in reference 1 that crack propagation rate (measured as the percentage of initial tension area failing per cycle) is constant for a large part of the total life.

7. CONCLUSIONS

From the present data the following conclusions concerning Mustang wing structures may be drawn:

(a) There are six distinct types of failure leading to final collapse. Failure type I occurs at station 80 in the tension skin, being initiated from an ammunition ejector chute cut-out. Failure types II to V all occur in the region of the tank-bay between stations 6 and station 33 and are propagated through the tank-bay door. Failure type VI occurs only in preloaded specimens and is initiated by a failure in the upper surface from the corners of the gun-bay near station 80.

(b) The relative frequency of occurrence of the gun-bay failure (type I) and the tank-bay failures (types II, III, and V) varies with the load range but is independent of the magnitude of the alternating load.

(c) The rate of crack propagation at the major failures (percentage of initial tension area failing per cycle) is approximately constant for a large part of the life (figs. 14 and 15).

(d) Lines of constant life drawn on the alternating load-mean load diagram are of the same general shape as those obtained for notched aluminium alloy specimens (fig. 24).

(e) When compared at the same nominal stress and load range ratio $R = 0$, the fatigue life to final failure corresponds to that of notched specimens of 24 ST alclad (the main material of construction) with a

theoretical stress concentration factor (K_T) of approximately 3.6. For riveted structures of sheet and stringer construction, correspondence with the notched material can be expected at a value of the theoretical stress concentration factor greater than 3.0.

(f) The frequency distribution of fatigue life is approximately logarithmic normal. There is evidence to show that this is true in general for structures of this type (appendix IV).

(g) For a given value of pre-load the relative increase in fatigue life is a function of the maximum load of the cycle only (fig. 28) and progressively increases as the maximum load is decreased until finally the life is prolonged until failure is initiated in the upper surface.

(h) There is an optimum value of pre-load which causes a maximum relative increase in life for all load ranges. This optimum pre-load is approximately 85 percent U.F.L. and results in a relative increase in life of over 300 percent when the maximum load of the cycle is below 30 percent U.F.L.

(i) In determining the fatigue strength of the critical component of a redundant structure, the local stress is affected by the force distribution between adjoining members, and the usual design methods do not allow for this refinement.

8. FUTURE WORK

Additional investigations proposed in the current programme are:

(a) Correlation between the fatigue characteristics of Mustang wings and notched specimens of 24 ST and 24 ST alclad.

(b) Determination of the reduction in fatigue life of Mustang wings that have seen long service.

(c) Investigation of load redistribution in the critical areas under various values of pre-load.

Investigations proposed following the present programme are:

(a) Cumulative damage tests on Mustang wings under various types of load sequence and application of a proposed Airworthiness Fatigue Test.

(b) Determination of the fatigue characteristics of an araldite bonded structure and comparison with an identical structure of riveted construction.

(c) Correlation between fatigue data of complex structures and notched test specimens (ref. 16).

(d) Correlation between laboratory tests such as reported above and actual service conditions (ref. 17).

9. ACKNOWLEDGEMENT

The authors wish to acknowledge the valuable support given to the project by W. W. Johnstone, Officer in Charge of Structures and Materials Experiment Group, and to express their appreciation to I. S. Milligan, D. G. Ford, J. G. Robertson, M. Rice, D. Gibson, S. Gee and G. Parry-Jones, without whose efforts as a team this work would not have been possible.

Department of Supply
Research and Development Branch
Aeronautical Research Laboratories
Melbourne Australia, January 1955

APPENDIX I

VIBRATION LOADING TEST METHOD

This method is a development of that used in the series of tests on CA-12 wings described in reference 15.

As shown in the general view of figure 8 the wing is inverted and attached at the fuselage connections to rolled steel joist supporting beams which span between reinforced concrete columns from which the whole assembly is suspended on spring steel strips.

The present series of tests at a mean load of 6 percent ultimate failing load require no externally applied steady load and therefore no loading frames are attached to the wing except at station 145 where the exciting force of the vibration is applied on the port side.

The method of fixed suspension is used to provide correct loading throughout the span. In this method the nodal points of the vibration are positioned by fixing the wing at the fuselage connections thus introducing the required alternating reactions at these points.

However the flexibility of the supporting beams has been designed to allow a bodily oscillation of the wing such that the resultant deflections of the structure produce the required shear loading without the addition of any large masses to the structure.

This bodily oscillation is practically in phase with the wing vibration exciting it since it is a forced vibration of the wing on its mountings, and the natural frequency of this system has been made relatively high. To apply the torsional moment distribution additional alternating forces are necessary and to avoid loading frames, aileron and flap hinges on the trailing edge of the wing have been selected as suitable attachment points.

A mass or a spring of suitable stiffness is attached according to the sign of the torsional moment to be applied. Shear and torsion diagrams for the applied loading are shown in figure 16 and a brief description of the method of calculation is given in appendix II.

The wing is excited on one side only which necessitates minimum bending restraint at the supporting points to obtain sympathetic vibration of the other side. This is obtained by suspending the supporting rolled steel joists on flexible steel strips maintained in tension by hydraulic jacks applying a steady downward load, which exceeds the maximum alternating load. To ensure equality of loading on all of the four steel strips the

front and rear pairs are each connected by a short beam pivoted at the centre on the main supporting columns.

Rolling of the wing about these pivots at low frequency during starting is restrained by rubber damping blocks. A view of the arrangement can be seen in figure 10 which shows the rear support assembly.

The tensioning jacks for the steel strips are supplied with oil at constant pressure from an hydraulic pump. This also supplies through a pressure regulator, a series of tension jacks which apply a constant load to the springs attached to the trailing edge of the wing in order to correct the torsional moment as described above.

The vibration is excited by a mechanical stroking machine driving the wing through a pair of stiff springs at station 145 on the port side. To provide a counter balance for the mean spring tension of the exciter springs a similar spring system is connected at a corresponding position on the starboard side.

The magnitude of the driving force is adjusted by altering the throw of the stroking machine, while speed control is obtained by using a D. C. motor drive powered by a 10 H.P. Ward Leonard set. After the throw of the stroking machine is set, according to the degree of excitation required, the D. C. Motor is started and the speed increased until a vibration is maintained just below the resonant frequency. The power input to the driving motor is then adjusted to obtain the desired amplitude of vibration as shown by a deflection indicator similar in principle to that described in reference 15 except that the body of the instrument is left free to "float" to the mean position of vibration. This is necessary since the wing is able to roll about the central supporting pivots.

A sketch of the device is shown in figure 11. It consists of an oil dash pot containing two pistons, one being fixed in space and the other being contacted by an upper striker attached to the wing. The cylinder of the dash pot is free to move on the fixed piston and is contacted by a lower striker on the wing. The oscillating strikers are thus continually holding piston and cylinder together against the pressure of a light spring. The cylinder carries a moveable contact between upper and lower fixed contacts and in the correct running position the moveable piston maintains the centre contact midway between the fixed contacts. Any change in amplitude causes the centre contact to close with the lower or the upper contact. This operates pilot lamps on the control desk and relays may be set if desired to switch off the generator set automatically. However after being initially set the vibration remains constant over long periods without further attention.

The accuracy of loading has been checked using electric resistance strain gauges and by measuring deflections at various points along the

span. These show that the maximum error in stress between any station from 0 to 100 does not exceed ±5 percent. (It is believed that the actual error is somewhat less than ±5 percent as this figure includes instrument errors.)

Investigation is proceeding into the effect of variation in load as the main failure develops but initial tests indicate that it does not cause a significant error in life. Specimens are run in the rig until failure is imminent. A number of such specimens have been loaded to final collapse in the hydraulic loading rig and have failed at practically the maximum load of the cycle.

APPENDIX II

CALCULATION AND VERIFICATION OF THE VIBRATION MODE

Consider each half of the wing to be divided into n segments and adopt the following notation.

m_r the mass of the r^{th} segment from the wing tip.

I_r moment of inertia of the r^{th} segment about its C.G.

x_r, y_r co-ordinates of the C.G. of the r^{th} segment relative to axes perpendicular and parallel to the span.

z_r amplitude of vibration of the C.G. of the r^{th} segment.

θ_r amplitude of rotation of the r^{th} segment about its C.G. [with respect to the y axis.]

ω frequency in rads/sec.

F_r amplitude of shear force due to m_r.

T_r amplitude of torsional moment exerted by the r^{th} segment about the y axis.

$f_r = \frac{F_r}{\omega^2}$ shear coefficient.

$t_r = \frac{T_r}{\omega^2}$ torque coefficient.

If the wing is in steady vibration at a frequency ω, then

$$F_r = m_r z_r \omega^2$$

and if the natural frequency in torsion is high relative to ω

$$T_r = \left(m_r z_r x_r + I_r \theta_r\right)\omega^2$$

For a resonant vibration in the prescribed mode the deflections z_r and θ_r must correspond to the deflected curve under the required loading and F_r and T_r are given by the shear and torsion diagrams.

Therefore to satisfy (1) and (2) for all values of r the mass distribution of the wing must in general be modified by attaching masses in a given position. The disadvantage with this procedure is that near the

fuselage connections the deflections z_r are very small and the masses m_r have to be correspondingly large involving the clamping of heavy weights to the structure.

To overcome this a method has been evolved in which a free bending vibration of the wing is excited but the forces at the fuselage connections, reacting the vibration, are allowed to force a vertical oscillation of the structure on its mountings. If the natural frequency of this mode is relatively high the oscillation will be practically in phase with the vibration producing it. This requirement obviously limits maximum amplitude of oscillation that can be permitted.

Let z_0 and θ_0 be the amplitudes of vertical oscillation and pitch of the whole structure on its mountings.

The resultant vibration of the r^{th} segment is then

$$z_r' = z_r + z_0 + x_r\theta_0 \tag{3}$$

$$\theta_r' = \theta_r + \theta_0 \tag{4}$$

This provides finite deflections in the neighbourhood of the fuselage connections and is the mode of vibration used in the present series of tests.

Each side of the wing was cut into 10 segments and the mass, moment of inertia about the y axis and position of the center of gravity were determined for each segment. The values of z_r and θ_r were obtained from a calibration in the hydraulic loading rig and the shear and torsion increments required at each segment were obtained from figure 16.

The shear coefficients are given by[3]

$$\begin{aligned} f_r &= m_r z_r + m_r z_0 + m_r x_r \theta_0 \\ &= m_r z_r + z_0 \left(m_r + m_r x_r \frac{\theta_0}{z_0} \right) \end{aligned} \tag{5}$$

---

[3]NACA reviewer notes that table III, column (9), suggests an alternate equality, as follows:

$$f_r = m_r z_r + m_r z_0 (1 + \alpha\, x_r), \text{where } \alpha = \frac{\theta_0}{z_0}$$

The value of $\frac{\theta_0}{z_0}$ is fixed by the position of the wing on its mounting beams. It is not feasible to alter this appreciably.

The shear coefficients were obtained from (5) and by suitably selecting the value of z_0 it was possible to approximate the form of the shear diagram closely without the addition of any masses. (See fig. 16.)

The value of ω was then obtained from the relationship

$$\omega^2 = \frac{F_r}{f_r} \tag{6}$$

The torsional increments due to each segment were then obtained as follows -

$$T_r = \left(m_r x_r \left[z_r + z_0 + x_r \theta_0\right] + I_r \theta_r\right)\omega^2 \tag{7}$$

These were plotted on the torsion diagram (see fig. 16) giving a nose down torsional moment generally in excess of that required. Correcting torques were therefore introduced at suitable stations. The aileron and flap hinges were selected as convenient attachment points and masses or springs of suitable stiffness as shown in Table IV were attached according to the sign of the torsional correction required.

These forces, of course affected the shear diagram but as they were relatively small a reiteration process using a modified value of z_0 was not necessary. The frame at station 145 enables a mass to be attached to effect any minor correction. The calculation of the shear and torsion coefficients is shown for the wing segments in table III and for the forces introduced to correct the torsion in table IV. The resulting shear and torsion diagrams are shown in figure 16 for the calculated value of frequency (ω = 13.4 c.p.s.).

A number of checks of the accuracy of loading have been made using electric resistance strain gauges attached to the spars. Deflection measurements have also been obtained by clamping pencils to the structure at various points and drawing a board past them while the wing is vibrating. The small deflections being forced at the fuselage connections have been measured with a Vibrograph.

The results of the most comprehensive of these tests are shown in detail in tables V and VI and indicate that at any point on the span the error in applied load is less than ±2 percent of the ultimate failing load. This is within the accuracy of measurement of the methods used to determine the strains and the deflections.

All the available strain gauge readings from a number of specimens have been used to provide a more reliable estimate. For each strain gauge reading the ratio

$$\frac{\text{load corresponding to indicated strain}}{\text{average load for the specimen}}$$

has been determined and plotted against spanwise location as shown in figure 12. The values are distributed in a random manner about a straight line through the value 1.0, indicating again that the accuracy of loading is well within the accuracy of measurement.

The accuracy of load control by the deflection indicator (described in appendix I) has been determined from strain gauge readings and deflection measurements taken on specimens during test. In figure 13 the applied load obtained from such readings has been plotted for a number of specimens against the load setting of the deflection indicator.

From the above results it is concluded that between station 0 and station 100 in. at least, the required stress distribution is obtained with an accuracy of ±5 percent or less.

APPENDIX III

DESCRIPTION OF MAJOR FAILURES

Type I - Failure at Station 80 Through the Ammunition Chute Cut-Out (Figures 5, 17, and 18)

This failure is initiated from a stress concentration at the corner of the ammunition chute cut-out in the neighbourhood of a drastic change in section of the tension skin. The tank-bay door load is taken out into a heavy doubling plate connected to the rib at station 75. This doubling plate extends out to station 80 (see figs. 5 and 18) surrounding the inboard half of the cut-out. The initiation of the failure is from the last rivet hole attaching stringer and skin to the doubling plate. The stress in the skin obviously rises steeply at this point where the doubling plate ends and this, combined with the stress round the hole near the edge of the cut-out, causes early appearance of a crack from the rivet hole to the cut-out. This crack then extends forward in the skin towards the front spar. A crack is also initiated at a later stage from the rear of the cut-out at a corresponding rivet hole or sometimes from the outboard corner of the cut-out since the hole is further from the edge of the cut-out in this case.

The stringer in front of the cut-out then fails either at the last rivet hole attaching it to the doubling plate or at the joggle at the outboard edge of the plate where there is considerable bending load in the stringer. The rear stringer then fails in a corresponding position (see fig. 18). Both these cracks are propagated across the tension skin through the outboard row of holes in the doubling plate causing progressive failures of stringers. The crack from the front of the cut-out reaches the front spar and is then propagated into the spar flange. This continues until failure occurs under maximum load of the cycle.

Type II - Failure at Station 21 Through the Tank Bay Door

Subsidiary cracks may appear from screw holes in the leading edge of the tank bay door where it is screwed to the front spar flange. These screw holes often coincide with spot welds (which attach the leading edge stringer to the door), and these are usually the sources of such subsidiary cracks.

A triangular panel forming the skin, rear of the wheel well (see figs. 4 and 5) is attached to the forward edge of the front spar by a row of rivets ending in 7 screws as the panel tapers out at station 21.

This panel transmits considerable tension load to the front spar flange, and the change in section where it ends at station 21 makes this area critical.

Failure is initiated from one of the subsidiary cracks occurring in the neighbourhood and is propagated into the front spar flange at an adjacent screw hole. This in turn increases the tension load in the tank bay door and the subsidiary crack extends rearward through the door while the crack in the spar flange progresses and extends down the web. (See fig. 19.) This leads to final collapse.

Type III - Failure at Station 28 Through the Tank Bay Door (Fig. 19)

In some cases the screws attaching the triangular skin panel to the front spar fail. If this happens all the load from the panel is transmitted to the front spar through the rivets further outboard. The stress round the end rivets in this region is therefore considerably increased and there is also a sudden change in section of the front spar flange where a doubler ends at station 28. This produces a major stress concentration and a failure develops combining with one of the subsidiary failures in the tank bay door referred to in type II.

The failure extends rearward through the tank bay door and also through the spar, as in type II, leading to final failure.

Type IV - Failure at Station 6 Through the Tank Bay Door (Fig. 20)

The joint cap covering the centre joint in the lower surface of the wing is attached to the tank bay door on each side by a line of anchor nuts 4 in. from the wing centre-line at approximately 6 in. pitch. No load is applied through these bolts holes but together with the two adjacent rivet holes attaching the anchor nut they cause a severe stress concentration. The tension load in the tank bay door causes a crack to appear between these holes. The failure then spreads fairly rapidly from each of the end holes and is propagated across the tank bay door. As the failure spreads (see fig. 20) the centre joint becomes ineffective and the tension load is redistributed into the front spar flange, the load being carried across the centre by the heavy fish plate joining the port and starboard spar flanges at the centre line. As the front spar now carries almost the entire tension load, failure develops rapidly either at station 21 where the spar doubler ends or near station 4 through the fish plate joint.

This type of failure has only been observed at low alternating loads (±11 percent U.F.L.) where the number of cycles is very great.

Type V - Failure in Region of Station 37 Through the Tank Bay Door

The triangular skin panel rear of the wheel well is joined to the forward edge of the front spar flange and has a heavy reinforcing plate attached where it tapers down between station 37 and station 21 (see fig. 4). A large part of the load in the skin panel is transferred to the main spar through this doubling plate. If no failure occurs in the spar this results in the rivets and screws between station 21 and station 37 failing successively. The stress concentration at station 21 is therefore transferred to the neighbourhood of station 37, particularly as the last rivets to fail in this area are transferring an increasing high local load to the spar.

The result is a failure in the spar flange very often through the last rivet attaching the reinforcing plate and the skin panel. This usually combines with one of the subsidiary cracks in the spot welds and the failure extends through the tank bay door and the front spar flange causing final collapse.

Type VI - Failure Introduced in Upper Surface at Station 77

This type of failure occurs only in pre-loaded specimen subjected to fluctuating loads the mean value of which is low (6 percent U.F.L. in specimens tested), and is due to the unfavourable stress distribution induced in the upper surface near the corners of the gun-bay. The rib at station 75 between the tank-bay and gun-bay is fitted with a heavy rib cap which interrupts the main spar flange between station 77 and station 73 in both the upper and lower surfaces of the wing.

A crack first appears in the skin at the forward inboard corner of the gun-bay at station 77, and then extends into the spar flange where it is cut out for the rib cap. This leads to a crack in the spar doubler also and the failure spreads down the web of both until it is arrested by a screw hole. The flange reinforcing plate fails and load is redistributed into the rear spar. In conjunction with the unfavourable stress distribution due to pre-loading this causes a failure in the upper spar flange of the rear spar at the outboard corner of the gun-bay. This failure extends both into the upper skin and down the spar web. (See fig. 21.)

The next stage is the development of a failure in the lower surface at station 73 at the interruption in the lower flange of the main-spar due to the rib at station 75 as explained above. The crack spreads into the spar doubler and down the web of each, until it reaches an inspection hole. The flange reinforcing plate fails in fatigue leaving the tension load to be carried by the tank-bay door and the skin panel covering the wheel well forward of the front spar.

Failure develops rapidly in the skin panel immediately inboard of the crack in the spar. There is a heavy reinforcing plate attached to the skin panel in this area and as the first crack spreads across the skin a second crack develops parallel to it along the inboard edge of the reinforcing plate as shown in figure 22.

The tank-bay door now carries all the load in this area and a crack develops rearward along the line of screws attaching it to the rib cap at station 75. This is followed by general failure of the tension skin through the inboard ammunition chute cut-out (fig. 23).

APPENDIX IV

STATISTICAL ANALYSIS OF THE DATA

1. Statistical Destribution of the Life to Final Failure

The data on pre-loaded specimens have been rejected as they are not necessarily representative of the population and also the result from specimen 20, which provides only one value at the particular load range. All other tests results have been included. The frequency distribution of fatigue life has been compared with the log normal distribution, following results obtained on simple specimens (refs. 5 and 12).

Let

n = Number of specimens tested at a given load range

N = Number of cycles to final failure of any specimen

$x = \log_{10} N$

$\bar{x} = \frac{\Sigma x}{n}$ the mean value of x at a given load range

$\bar{N} = \text{antilog } \bar{x} = \text{antilog} \left(\frac{\Sigma \log N}{n} \right)$, the mean life at a given load range, established on a logarithmic basis.

$S = \sqrt{\frac{\Sigma (x - \bar{x})^2}{n - 1}}$ the standard deviation of the n values of x.

The standardised variate $\delta = \frac{x - \bar{x}}{S}$ has been calculated for every specimen at each load range. The value of $\bar{x}$ has been obtained from the constant life lines of figure 24 which are drawn for $\bar{N}$ the logarithmic mean of the life. The value of S at any load range has been similarly determined from an alternating load - mean load diagram showing lines of constant standard deviation. The reason for this procedure was to reduce the error involved in estimating the mean and particularly the standard deviation from the small number of results available at each load range.

The cumulative distribution of δ is plotted in figure 32 and, except at extreme values, shows good agreement with the straight line representing the standardised normal variable. This shows that the logarithm of the fatigue life to final failure is approximately normally distributed.

By purely theoretical reasoning Freudenthal has shown (ref. 5) that for simple specimens a logarithmic normal distribution can be expected to give a good approximation to the distribution of the fatigue life at any particular stress level. He considers an applied alternating stress of constant amplitude to result in randomly varying stresses S_1 S_2 . . . S_k at any point in the material, the variation in the local stress being due to "density fluctuations and place changes of particles" resulting from the continual atomic and sub-atomic movement within the material.

Under any stress S_{k+1} the increase in the area of disruption A_k is regarded as being proportional to the stress cycle and to some function $f(A_k)$ of the disrupted area, which represents the effect due to progressive damage.

Thus

$$\left(A_{k+1} - A_k\right) = S_{k+1} f(A_k) \tag{1}$$

$$\therefore S_{k+1} = \frac{A_{k+1} - A_k}{f(A_k)}$$

and hence

$$\sum_{0}^{n} (S_k) = \sum_{0}^{n-1} \left(\frac{A_{k+1} - A_k}{f(A_k)} \right) \approx \int_{A_0}^{A_{n-1}} \frac{dA}{f(A)} \tag{2}$$

Freudenthal proposes the simple approximation:

$$f(A_k) = CA_k \qquad C = \text{a constant}$$

Then

$$\sum_{0}^{N}(S_k) \approx \frac{1}{C} \log \frac{A_N}{A_0} \tag{3}$$

He then shows that, using the Central Limit Theorem, the L.H.S. [left hand-side] of (3) tends to a normal distribution and that this leads to a log normal distribution for the cycles to failure N.

In the life to final failure of a large structure there is a long period of crack progagation as will be seen from figures 14 and 15. During this period conditions ahead of the crack may be represented by Freudenthal's model if the function $f(A_k)$ includes all effects that occur in the structure such as load redistribution and progressive increase in the nominal stress. The assumption, that $f(A_k) = CA_k$ under these conditions, has been tested from observed crack propagation rates in the Mustang wing.

Considering the progress of damage over a large number of cycles from N_0 to N_k,

$$\sum_{N_0}^{N_k} S_k = (N_k - N_0)S_{N_k} \tag{4}$$

S_{N_k} being the mean value of the random variables S_0, $S_1 \ldots S_K$. For any given value of N_k (provided $N_k - N_0$ is large) $\sum_{N_0}^{N_k} S_k$ and hence $(N_k - N_0)\ S_{N_k}$ is normally distributed about a mean value $(N_k - N_0)\mu_k$. Therefore if corresponding to given N_k and N_0, average values of S_{N_k}, A_{N_k}, and A_{N_0} are taken over a number of specimens we may take the mean value of $\bar{S}_{N_k}$ as an estimate of μ_k.

Then from (3) and (4)

$$\frac{1}{C} \log \left\{ \frac{\bar{A}_{N_k}}{\bar{A}_{N_0}} \right\} = (N_k - N_0)\bar{S}_{N_k} \approx (N_k - N_0)\,\mu_k$$

Therefore

$$(N_k - N_0) \approx \text{Constant} \times \log \left\{ \frac{A_{N_k}}{A_{N_0}} \right\}$$

Values of A_{N_0}, $A_N \cdots A_{N_k}$ have been obtained from the length of the visible crack as failure progresses the damaged area ahead of the crack being assumed substantially constant. Since N_0 and A_{N_0} are constant log A_{N_k} has been plotted against N_k/N_f (where N_f is the life to final failure). This has been done for four types of failure and in each case the agreement with a straight line is reasonably good. The results are the average of four specimens and the intervals $A_2 - A_1$, $A_3 - A_2$, . . . are all fairly large including at least several hundred cycles.

This investigation shows that the rate of increase of the area of disruption is approximately proportional to the extent of the disrupted area, even during the propagation of a fatigue crack through a complex wing structure. This result can also be applied to the period of crack initiation, as Freudenthal has shown that it applies to simple specimens. Therefore Freudenthal's theoretical approach can be applied for final failure in a large structure and this further supports the log normal distribution as a useful approximation to the distribution of fatigue life.

2. Determination of an Alternating Load - Mean Load Diagram for Extreme Probabilities of Failure

From the frequency distribution of figure 32 the values of δ, for probabilities of failure P of 0.01 and 0.99, have been determined and used in conjunction with the A-M diagram of figure 24 and the A-M diagram of standard deviation, referred to above, to determine values of x and hence N corresponding to probabilities of failure of 0.01 and 0.99. This has enabled lines of failure for fairly extreme values of probability to be drawn as shown in figure 25. The procedure is given in detail in reference 11.

3. Dependence of Type of Failure on the Load Range

In unpreloaded specimens five distinct types of major failure have been observed and it is a matter of great interest to know whether the frequency of occurrence of the type of failure is significantly dependent on the load range. A preliminary investigation has been made using the present test data on unpreloaded specimens as shown in table VII.

Due to the relatively small number of occurrences of the failures it has been necessary to group some of them together to form a reliable basis for statistical analysis. Types II, III, and V have been considered as one type since their methods of initiation and propagation are similar. As there are only two failures of type IV in the present data it has been excluded from this investigation.

The effect on the type of failure of mean load, alternating load and maximum load of the cycle has been considered. The corresponding null hypotheses are designated H_1, H_2, H_3, and are as follows.

H_1 The frequencies of occurrence (ref. table VII) of failure type I and failure types II, III, and V are not significantly dependent on the mean load of the cycle.

H_2 The frequencies of occurrence of failure type I and failure types II, III, and V are not significantly dependent on the alternating load of the cycle.

H_3 The frequencies of occurrence of failure type I and failure types II, III, and V are not significantly dependent on the maximum load of the cycle.

Consider first hypothesis H_1. The data has been rearranged into a series of classes, each class containing data for load ranges, of substantially the same mean load as shown in table VIII. The expected frequencies are then obtained, by dividing the total occurrences for each class between each type of failure, in the ratio of their total number of occurrences for all the classes, as shown in columns 5 and 6. The X^2 test is then applied to determine the probability that the observed values accord with the expected values as calculated on the assumption that H_1 holds. The same procedure is then applied for H_2 and H_3 by selecting classes of the same alternating load and the same maximum load respectively. The values of X^2 and the corresponding significance levels are shown in columns 9 and 10 of table VIII.

The results indicate a highly significant value of X^2 for H_1 and H_3. For H_2 the class intervals of high alternating load necessarily tend to include load ranges with high maximum load and in view

of the result of the test on H_1 it is to be expected that this factor will influence the X^2 test on H_2. Since this has shown that H_2 is discordant with the data at the 5 percent significance level only, it appears safe to accept H_2. This is borne out by the similar results for the X^2 tests on H_1 and H_3 which would show some difference if there was any marked influence of alternating load.

It is therefore concluded that the relative frequency of occurrences of the two kinds of failure is dependent on some parameter of the load range, other than the magnitude of the alternating load. The data at present available is not sufficient to yield any more definite conclusion.

APPENDIX V

RELATION BETWEEN THE FATIGUE STRENGTH OF P51-D MAINPLANES AND NOTCHED 24ST ALCLAD

In the tension surface of the wing the main spar doubling plate, rear spar and skin are of 24ST alclad so that the life to final failure is mainly dependent on the fatigue properties of this material. Unfortunately few data are available on notched 24ST alclad but S-N curves for $R = 0$ at K_T values of 1.0, 2.0, and 5.0 (refs. 8 and 9) are shown in figure 29 and curves for any other K_T value can be obtained by interpolation.[4]

An alternating load - N curve for $R = 0$ has been obtained for the mainplanes, from figure 24 and plotted as an S-N curve in figure 30 (curve (a)) on the basis of the nominal stress in the tank bay as measured by strain gauges. A similar curve has been drawn (curve (b) in fig. 30) based on the nominal stress in the gun bay area.

At high mean loads (and therefore, since $R = 0$, high alternating loads) failure occurs in the gun bay area (type I), but at lower loads it occurs in the tank bay (types II, III, and V) as represented by the shaded areas in figure 30.

Using figure 29 [or 34] an S-N curve for 24ST alclad of appropriate K_T value has been plotted and this gives good agreement with the life of the wing for failures in both areas.

Therefore, although the area where final failure occurs is determined by the load range, it has been shown that, for $R = 0$ at least, the life of the wing is similar to that for 24ST alclad of an appropriate K_T value provided the comparison is based on the nominal stress in the area where failure occurs. An explanation for this result is suggested in appendix VI. where the general mechanism of final fatigue failure is discussed.

---

[4]NACA reviewer suggests that figure 34 may be used for this purpose.

APPENDIX VI

DESCRIPTION OF THE MECHANISM OF FATIGUE FAILURE

All specimens that were not pre-loaded followed a characteristic pattern in their life to final failure. As can be seen in figures 14 and 15 this failure occurs in 3 distinct stages:

(a) The stage leading to propagation of a visible crack which occupies from 20 percent to 50 percent of the total life.

(b) The period of practically constant rate of crack propagation, occupying from 20 percent to 30 percent of the life.

(c) The final stage in which the rate of propagation progressively increases. This stage occupies 20 percent to 40 percent of the total life and is characterised by a marked increase in the nominal stress and appreciable load redistribution in the structure.

In stage (a) the time for first appearance of a crack is dependent on the severity of the local stress concentration but the initial crack is usually arrested by a nearby rivet hole and stage (a) is regarded as being complete when the crack begins to progress. In all cases the initial crack starts from the outside edge of a hole near the edge of a relatively rigid member, usually where there is some other contributing cause, such as load diffusion round the ejector chute cut-out or spot welds in the tank-bay door. Stage (a) is therefore associated with a stress concentration similar to that at the outside edge of a hole near the edge of an infinite sheet. When the crack breaks through to the edge, the stress concentrator becomes a key-hole slot or, to a first approximation, a "U" notch. In either event the theoretical stress concentration factor is in excess of 3.0 (refs. 13 and 14) even assuming no effect from a bolt or rivet.

In stage (b) the failure is propagated through the main body of the structure. As the crack travels across the surface, load is redistributed into the stringer or stiffener immediately ahead of it through the neighbourhood rivets, and so the failure is led into the nearest rivet hole and progresses across the surface in this manner, spreading from one rivet hole to the next.

The theoretical stress concentration factor round each hole in the path of the failure will initially be approximately 3.0, since it corresponds to a hole remote from the edge of a semi-infinite sheet, (ref. 13) but after the crack enters it the stress concentration will rise considerably and propagate the crack. Therefore as long as the nominal stress in the tension surface is substantially constant the rate of progress can

be expected to be fairly uniform and correspond to fatigue failure in the notched material at a theoretical stress concentration factor above 3.0. This has been investigated using constant rates of crack propagation "r" determined from figures 14 and 15. A life of $N_e = \frac{1}{r}$ has been obtained corresponding to failure of the whole tension area at the constant rate r. This can be regarded as the life of a notched specimen having a stress concentration factor equivalent to that which produces the constant rate of failure r in the wing, under the nominal alternating stress f_a of the load range.

To enable the notched 24ST alclad data of figure 29 to be applied, the A-M diagram of figure 24 has been used to give for the life N_e an alternating stress f_a at $R = 0$, corresponding to the alternating stress f_a at the test load. Using the f_a and N_e so obtained the corresponding value of K_T is determined from figure 34. The results for specimens 31-32, 71-72, and 90 are shown in table IX, these being the only specimens available that were tested near $R = 0$. All the results are reasonably close to $K_T = 3.0$.

During the final stage (c) the effect of increase in nominal stress, and load redistribution in the structure, accelerates the rate of failure, in addition to the fact that the material has already suffered considerable fatigue damage. Eventually, force redistribution in the structure outweights all other factors until static failure occurs under the maximum load of the cycle. The equivalent stress concentration factor related to the original value of the nominal stress becomes very high.

This does not claim to be more than a general picture of the mechanism of final fatigue failure, but it suggests that in a structure of this type (riveted sheet and stringer construction) fatigue failure develops under conditions corresponding to a theoretical stress concentration factor of 3.0 or more. In appendix V the life to final failure of Mustange wings at load range ratio $R = 0$ (including failure types I, II, III and V) has been found to approximate that of 24ST alclad for a theoretical stress concentration factor of 3.6.

REFERENCES

1. Johnstone, W. W., and Payne, A. O.: Determination of the Fatigue Characteristics of "Mustang" P51D Wings. A.R.C.C.30.

2. Wing Analysis for Model P51D Airplane Report No. 5891, North American Aviation Inc. Inglewood. July, 1944.

3. Johnstone, W. W., and Patching, C. A.: Static Strength Tests on "Mustang" P51D Wings. S. & M. Note 185, A.R.L. Department of Supply, Melbourne.

4. Patching, C. A.: Interim Note on Repeated Load Testing of Mustang P51D Wings. S. & M. Note No. 189, A.R.L. Department of Supply, Melbourne.

5. Freudenthal, A. M.: Planning and Interpretation of Fatigue Tests. Symposium on Statistical Aspects of Fatigue. A.S.T.M. - S.T.P. No. 121.

6. Grover, H. J., Bishop, S. M., and Jackson, L. R.: Axial load Fatigue tests on Notched Sheet Specimens of 24S-T3 and 75S-T6 Aluminium Alloys and of S.A.E. 4130 Steel with Stress concentration factors of 2.0 and 4.0. NACA TN 2389, 1951.

7. Grover, H. J., Bishop, S. M., and Jackson, L. R.: Axial load Fatigue tests on Notched Sheet Specimens of 24S-T3 and 75S-T6 Aluminium alloys and of S.A.E. 4130 Steel with stress concentration factor of 5.0. NACA TN 2390, 1951.

8. Lundberg, B. K. O., and Wållgren, G. G. E.: A study of some factors affecting the fatigue life of aircraft parts with application to structural elements of 24ST and 75ST Aluminium Alloys. Flygtekniska Forsöksanstalten Report No. 30 (Sweden).

9. Hartman, A.: Investigation of the notch sensitivity of 24ST and 75ST Alclad under alternating tension. National Luchtvaartlaboratorium Report No. 1819 (Amsterdam).

10. Weibull, W.: A statistical representation of fatigue failures in solids. Transactions of the Royal Institute of Technology Stockholm, Sweden No. 27, 1949.

11. Ford, D. G., and Payne, A. O.: A Statistical Analysis of Fatigue Data on a Typical Metal Wing. S. M. Report in course of preparation.

12. Head, A. K.: Statistical Properties of Fatigue Data on 24 ST Aluminium Alloys. S. & M. Note 180 A.R.L. Dept, of Supply, Melbourne.

13. Mindlin, R. D.: Stress Distribution around a hole near the edge of a plate under tension. Proc. Soc. Ex. Stress An., Vol. 5, No. 2, 1948, pp. 56-68.

14. Heywood, R. B.: Designing by Photo-Elasticity. 1952, p. 162.

15. Johnstone, W. W., Patching, C. A., and Payne, A. O.: An Experimental Determination of the Fatigue Strength of CA-12 "Boomerang" Wings. Report S.M. 160 A.R.L. Dept. of Supply, Melbourne.

16. Johnstone, W. W., Mann, J. Y., and Payne, A. O.: Fatigue Projects in connection with the prediction of the Life of Aircraft Structures from Tests on simple specimens, joints and fittings. S. M. Projects F 28/10, F 28/11 and F 28/12. A.R.L. Melbourne, May 1952.

17. Johnstone W. W., and Moody, E. S.: Fatigue equipment for simulating the flight stresses of Aircraft. Report S.M. 296. A.R.L. Melbourne, June 1953.

TABLE I

FATIGUE TEST RESULTS ON P-51 D "MUSTANG" SEMI-MAINPLANE

[All specimens other than those mentioned have a service life less than 500 hours. Odd specimen nos. - port halves. Even specimen nos. - starboard halves.]

Spec. no.	Load range		Type of failure	Cycles to failure		Test rig. (a)	Remarks
	Mean ld., % U.F.L.	Alt. ld., % U.F.L.		Initial failure	Final failure		
(1)	(2)	(3)	(4)	(5)	(6)	(7)	(8)
71	6	10.6	IV	990,600	1,807,200	V	
72	"	"	III	748,600	1,605,100	V	
81	"	"	IV	680,000	970,000	V	
82	"	"	I	638,000	1,231,000	V	
83	"	"	V	350,000	1,145,000	V	
84	"	"	I	550,300	1,395,000	V	
87	"	"	V	110,000	1,295,000	V	
88	"	"	V	50,000	1,401,000	V	
89	"	"	I	169,300	1,098,100	V	
90	"	"	II	169,300	796,700	V	
127	"	"	V	51,100	4,448,000	V	Pre-load 95% Service life 1,061 hours
128	"	"	V	51,100	5,219,000	V	Pre-load 95% Service life 1,061 hours
137	"	"	III	141,300	4,016,000	V	Pre-load 94% Service life 615 hours
140	"	"	VI	141,300	4,769,000	V	Pre-load 85%
63	6	16.6	III	49,100	216,000	V	
64	"	"	III	82,000	174,000	V	
67	"	"	II	35,800	106,000	V	
68	"	"	I	25,800	178,000	V	
75	"	"	III	29,100	193,000	V	
76	"	"	II	185,000	530,000	V	

[a] V Denotes tested in vibration rig.
H Denotes tested in hydraulic rig.
* Denotes specimen retained for further testing.

TABLE I.- Continued

FATIGUE TEST RESULTS ON P-51 D "MUSTANG" SEMI-MAINPLANE

[All specimens other than those mentioned have a service life less than 500 hours. Odd specimen nos. - port halves. Even specimen nos. - starboard halves.]

Spec. no.	Load range		Type of failure	Cycles to failure		Test rig. (a)	Remarks
	Mean ld., % U.F.L.	Alt. ld., % U.F.L.		Initial failure	Final failure		
(1)	(2)	(3)	(4)	(5)	(6)	(7)	(8)
85	6	16.6					*
86	"	"	V	84,100	301,600	V	
93	"	27.5					*
94	"	"	I	6,400	24,700	V	
99	"	"	III	1,800	12,200	V	
100	"	"	I	1,800	15,600	V	
117	"	"					* Pre-load 85% Service life 539 hours
118	"	"	V	5,000	72,100	V	Pre-load 85% Service life 539 hours
119	"	"					* Pre-load 85% Service life 873 hours
120	"	"	I	0	85,300	V	Pre-load 85% Service life 873 hours
91	"	"					*Pre-load 90%
92	"	"	I	6,600	58,600	V	Pre-load 90%
111	"	"	III	10,000	68,600	V	Pre-load 90%
112	"	"	I	29,600	75,400	V	Pre-load 90%
103	"	"					* Pre-load 95%
104	"	"	I	4,000	21,500	V	Pre-load 95%
113	"	"					* Pre-load 95%
114	"	"	I	20,000	66,200	V	Pre-load 95%
143	"	"					* Pre-load 70%
144	"	"	I	47,100	68,100	V	Pre-load 70%
145	"	"					* Pre-load 70%
146	"	"	III	10,000	11,500	V	Pre-load 70%

[a] V Denotes tested in vibration rig.
H Denotes tested in hydraulic rig.
* Denotes specimen retained for further testing.

TABLE I.- Continued

FATIGUE TEST RESULTS ON P-51 D "MUSTANG" SEMI-MAINPLANE

[All specimens other than those mentioned have a service life less than 500 hours. Odd specimen nos. - port halves. Even specimen nos. - starboard halves.]

Spec. no.	Load range		Type of failure	Cycles to failure		Test rig. (a)	Remarks
	Mean ld., % U.F.L.	Alt. ld., % U.F.L.		Initial failure	Final failure		
(1)	(2)	(3)	(4)	(5)	(6)	(7)	(8)
129	3	35	III	2,500	8,100	H	
130	"	"	III	500	5,948	H	
131	"	"	III	1,070	5,250	H	
132	"	"	III	686	3,914	H	
105	16	24	I	2,160	22,000	H	
106	"	"	V	4,090	17,859	H	
107	"	"	I	3,135	17,900	H	
108	"	"	I	2,044	15,699	H	
115	"	"	I	1,595	12,300	H	Service life 547 hours
116	"	"	III	1,220	8,576	H	Service life 547 hours
133	"	"					* Service life 1,064 hours
134	"	"	I	0	14,609	H	Service life 1,064 hours
141	"	"					* Service life 1,071 hours
142	"	"	III	6,470	19,241	H	Service life 1,071 hours
147	"	"					* Service life 1,025 hours
148	"	"	III	7,030	10,914	H	Service life 1,025 hours
153	"	"					* Service life 1,073 hours
154	"	"	I	0	21,914	H	Service life 1,073 hours
95	16	35	III	475	2,829	H	
96	"	"	I	107	2,950	H	
97	"	"	II	1,758	3,506	H	
98	"	"	III	715	2,267	H	

[a] V Denotes tested in vibration rig.
H Denotes tested in hydraulic rig.
* Denotes specimen retained for further testing.

TABLE I.- Continued

FATIGUE TEST RESULTS ON P-51 D "MUSTANG" SEMI-MAINPLANE

[All specimens other than those mentioned have a service life less than 500 hours. Odd specimen nos. - port halves. Even specimen nos. - starboard halves.]

Spec. no.	Load range		Type of failure	Cycles to failure		Test rig. (a)	Remarks
	Mean ld., % U.F.L.	Alt. ld., % U.F.L.		Initial failure	Final failure		
(1)	(2)	(3)	(4)	(5)	(6)	(7)	(8)
101	16	35	V	1,530	3,514	H	
102	"	"	V	1,530	2,858	H	
27	24	13.4	II	44,404	54,307	H	
28	"	"	I	11,354	61,000	H	
31	"	"	I	2,019	42,000	H	
32	"	"	I	2,214	32,116	H	
39	30.1	12.9	I	0	70,406	H	
40	"	"	I	13,300	87,900	H	
43	"	"	I	11,630	77,400	H	
44	"	"	I	7,790	68,273	H	
9	26.9	16.1	I	3,221	28,187	H	
10	"	"	I	4,774	29,400	H	
11	"	"	III	30,092	35,725	H	
12	"	"	III	17,615	31,084	H	
17	"	"	I	3,205	47,249	H	
18	"	"	III	4,200	17,115	H	
29	"	"	III	0	62,494	H	Pre-load 85.6%
30	"	"	V	3,675	82,000	H	Pre-load 85.6%
47	"	"					*
							Pre-load 85.6%
48	"	"	III	20,750	44,973	H	Pre-load 85.6%
121	"	"	V	1,970	65,320	H	Pre-load 95%
122	"	"	III	18,550	52,990	H	Pre-load 95%
123	"	"	V	20,800	53,930	H	Pre-load 95%
124	"	"					*
							Pre-load 95%
19	29.6	18.8					*
20	"	"	III	3,590	13,118	H	
65	32	40	I	20	727	H	
66	"	"	V	617	766	H	
69	"	"					*
70	"	"	V	550	550	H	Initial failure not observed

[a] V Denotes tested in vibration rig.
H Denotes tested in hydraulic rig.
* Denotes specimen retained for further testing.

TABLE I.- Continued

FATIGUE TEST RESULTS ON P-51 D "MUSTANG" SEMI-MAINPLANE

[All specimens other than those mentioned have a service life less than 500 hours. Odd specimen nos. - port halves. Even specimen nos. - starboard halves.]

Spec. no.	Load range		Type of failure	Cycles to failure		Test rig. (a)	Remarks
	Mean ld., % U.F.L.	Alt. ld., % U.F.L		Initial failure	Final failure		
(1)	(2)	(3)	(4)	(5)	(6)	(7)	(8)
5	32.3	21.5	V	2,824	8,693	H	
6	"	"	III	2,824	4,936	H	
13	"	"	II	4,748	10,379	H	
14	"	"	III	2,165	7,812	H	
4	"	"	III	3,755	12,971	H	Pre-load 103%
15	37.7	26.9	I	670	3,300	H	
16	"	"	I	670	2,441	H	
21	"	"	I	150	5,400	H	
22	"	"	I	1,181	4,926	H	
33	"	"	I	257	5,200	H	Pre-load 85.5%
34	"	"	III	1,786	4,895	H	Pre-load 85.5%
35	"	"	I	494	5,000	H	Pre-load 85.5%
36	"	"	I	728	4,799	H	Pre-load 85.5%
125	"	"	I	1,034	4,400	H	
126	"	"	V	1,435	4,362	H	
37	45.2	19.4	I	2,275	14,564	H	
38	"	"	I	2,396	14,900	H	
41	"	"	I	2,230	12,400	H	
42	"	"	I	1,600	11,175	H	
59	"	"	I	30	13,400	H	
60	"	"	II	5,060	10,619	H	
55	47	11	II	45,270	56,745	H	
56	"	"					*
57	"	"	II	47,082	65,091	H	
58	"	"					*
61	"	"	I	5,664	100,000	H	
62	"	"	II	77,515	98,066	H	
77	"	"	I	12,775	83,500	H	
78	"	"	I	12,775	76,012	H	
79	"	"					*
80	"	"	I	4,672	56,863	H	

[a] V Denotes tested in vibration rig.
H Denotes tested in hydraulic rig.
* Denotes specimen retained for further testing.

TABLE I.- Concluded

FATIGUE TEST RESULTS ON P-51 D "MUSTANG" SEMI-MAINPLANE

[All specimens other than those mentioned have a service life less than 500 hours. Odd specimen nos. - port halves. Even specimen nos. - starboard halves.]

Spec. no.	Load range		Type of failure	Cycles to failure		Test rig. (a)	Remarks
	Mean ld., % U.F.L.	Alt. ld., % U.F.L.		Initial failure	Final failure		
(1)	(2)	(3)	(4)	(5)	(6)	(7)	(8)
51	47	24	I	860	4,550	H	
52	"	"	II	460	4,443	H	
53	"	"	I	310	4,560	H	
54	"	"	I	496	4,391	H	
73	"	"	I	394	5,000	H	
74	"	"	III	3,565	4,780	H	
23	48.4	37.6					*
24	"	"	I	213	435	H	
25	"	"	I	39	634	H	
26	"	"	I	243	660	H	
45	68.25	12.1	I	4,650	34,000	H	
46	"	"	I	4,650	26,229	H	
49	"	"					*
50	"	"	III	2,095	24,648	H	

[a] V Denotes tested in vibration rig.
H Denotes tested in hydraulic rig.
* Denotes specimen retained for further testing.

TABLE II

EFFECT OF PRE-LOADING ON FATIGUE LIFE

Magnitude of pre-load, % U.F.L.	Load range, % U.F.L.	Mean life		Relative increase in life, %	Failure type virgin specimen	Failure type pre-loaded specimen
		Virgin specimen, cycles	Pre-loaded specimen, cycles			
85	6 ± 10.6	1,238,000	4,769,000	285	V	VI
95	"		4,561,000	268		III
70	6 ± 28	17,500	68,100	289	I	I
85	"		78,700	350		III
90	"		67,500	286		I
95	"		43,800	150		I
85	26.9 ± 16.1	31,460	63,820	103	I, III	III
95	"		57,410	82.5		III
103	32.3 ± 21.5	7,950	12,971	63	III	III
85.6	37.7 ± 26.9	4,139	4,975	20.2	I	I, III

TABLE III

SHEAR AND TORSION COEFFICIENTS VIBRATION LOADING RIG

Segment no.	Mass distribution of segment				Deflections at C.G.		Shear coeff. f_r			Torque coeff. t_r
	(2)	(3)	(4)	(5)	(6)	(7)	(8)	(9)	(10)	(11)
	y_r, in.	x_r, in.	m_r, lb.	I_r, lb.in.^{2}	z_r, in.	θ_r, rad.	$m_r z_r$, lb.in.	$m_r z_0(1 + \alpha x_r)$, lb.in.	Total fr, lb.in.	t_r, lb.in.^{2}
1	217	-8.8	7	1.2×10^3	0.97	10.8×10^{-5}	6.8	0.33	7.1	-63
2	202	-6.7	9	1.7	.86	19.4	7.7	.43	8.2	-56
3	176	-10.6	40	9.6	.67	35.2	26.8	1.9	28.7	-305
4	143	-11.1	46	12.9	.45	-29.8	20.7	2.14	22.8	-253
5	125	-10.2	22	5.9	.34	-25.0	7.5	1.19	8.7	-89
6	107	-8.2	52	13.1	.26	34.9	13.5	2.46	16.0	-132
7	88	-4.0	52	10.7	.19	64.0	9.9	2.65	12.6	-60
8	69	-3.5	180	32.0	.12	72.0	21.6	8.81	30.4	-109
9	43	-12.7	52	22.0	.055	35.0	2.9	2.38	5.3	-68
10	16	-17.8	124	58.0	0	0	0	5.51	5.5	-99

$z_0 = 0.051$ in. $\alpha = \frac{\theta_0}{z_0} = 0.006$ in.$^{-1}$ calculated value of $\omega = 13.4$ c.p.s.

$F_r = 19.6\ f_r$. $T_r = 19.6\ t_r$.

TABLE IV

SHEAR AND TORSION COEFFICIENTS DUE TO APPLIED FORCES VIBRATION RIG

y, in.	x, in.	z, in.	Mass, lb.	Spring stiffness, lb.in.	Shear coeff., f, lb.in.	Torque coeff., t, $lb.in.^2$	Remarks
(1)	(2)	(3)	(4)	(5)	(6)	(7)	(8)
166	-35.2	0.65		97	-3.15	+111	Spring at aileron hinge bracket
145	-16.7	0.53	18		+9.55	-159	Exciter frame
	-40.0	0.51		185	-4.73	+189	Spring at rear of frame
126	-37.0	0.40		150	-3.0	+111	Spring at flap hinge bracket
76	-43.5	0.15	21		+3.2	-139	Mass at flap hinge bracket

$(6) = (4) \times (3)$ $\qquad \omega = 13.4$ c.p.s.

or $\quad = \dfrac{(5) \times (3)}{\omega^2}$

TABLE V

STRAIN GAUGE READINGS - VIBRATION LOADING RIG

Specimen No. 63/64

Load Ranges: 6 ± 16.6% U.F.L.

Measured ω = 12.6 c.p.s.

Location	Type of strain	Gauge station	Indicated load	Deviation from mean value
(1)	(2)	(3)	(4)	(5)
Starboard Front spar	Compression	21 in.	17.1% U.F.L.	0.6% U.F.L.
	Tension	19	16.6	0.1
	Compression	65	16.5	0.0
	Tension	65	18.5	2.0
	Compression	97	16.5	0.0
	Tension	143	17.6	1.1
Starboard Rear spar	Tension	25	16.0	-0.5
	Tension	64	18.7	2.2
	Tension	97	15.1	-1.4
	Compression	132	13.4	-3.1
		Avg.	16.6	
Port Front spar	Tension	100.5	15.1	-1.4
Port Rear spar	Compression	63	15.9	-0.6
	Tension	63	17.5	1.0
	Compression	24	17.1	0.6
	Tension	24	15.8	-0.7
		Avg.	16.3	

Mean value of all readings = 16.5% U.F.L.
(5) = (4) - 16.5%

TABLE VI

DEFLECTION READINGS AT 25 PERCENT CHORD LINE

VIBRATION LOADING RIG

Specimen No. 63/64

Load Range: 3 ± 16.6% U.F.L.

Measured ω = 12.6 c.p.s.

Station	Deflection for 10% U.F.L. from calibration	Observed deflection	Corresponding alt. load, % U.F.L.	Deviation from mean value, % U.F.L.
(1)	(2)	(3)	(4)	(5)
117 in.	0.30 in.	0.46 in.	15.3%	-1%
145	0.445	0.75	16.9	+0.9
216	0.915	1.53	16.7	+0.7

Mean value = 16.3%.

(2). From deflection test in hydraulic loading rig.

(3). Deflection (referred to 25 percent chord line) as measured in vibration rig.

$$(4). = \frac{(3)}{(2)} \times 10.$$

(5). = (4) - 16.3%.

TABLE VII

DISTRIBUTION OF FATIGUE FAILURE TYPES

Load, % U.F.L.			Failure type					
Mean	Alt.	Max.	I	II	III	IV	V	II, III, and V
6.0	10.6	16.6	0	1	2	2	3	6
6.0	16.6	22.6	0	2	3	0	1	6
6.0	28.0	34.0	2	0	1	0	0	1
6.0	35.0	41.0	0	0	2	0	0	2
16.0	24.0	40.0	4	0	1	0	1	2
16.0	35.0	51.0	1	1	2	0	2	5
24.0	13.4	37.4	3	0	1	0	0	1
30.1	12.9	43.0	4	0	0	0	0	0
26.9	16.1	43.0	3	1	2	0	0	3
29.6	18.8	48.4	0	0	1	0	0	1
32.3	21.5	53.8	1	1	2	0	0	3
32.0	40.4	72.4	1	0	2	0	0	2
37.7	26.9	64.6	5	0	0	0	1	1
47.0	11.0	58.0	4	3	0	0	0	3
45.2	19.4	64.6	5	1	0	0	0	1
47.0	24.0	71.0	4	1	1	0	0	2
48.4	37.6	86.0	3	0	0	0	0	0
68.3	12.0	80.3	3	0	0	0	0	0

TABLE VIII

STATISTICAL ANALYSIS OF FAILURES

Hypothesis	Class interval of loads	Frequency of occurrence of failure					Degress of freedom	x^2	Signifigance level
		Observed		Expected		Total			
		I	II, III, V	I	II, III, V				
(1)	(2)	(3)	(4)	(5)	(6)	(7)	(8)	(9)	(10)
H_1	6-26.9	13	26	20.42	18.58	39			
Effect of	29.6-37.7	11	7	9.43	8.57	18	2	11.24	1%
Mean load	45.2-68.3	19	6	13.10	11.90	25			
		43	39			82			
H_2	10.6-13.4	14	10	12.58	11.42	24			
Effect of	16.1-18.8	3	10	6.82	6.18	13	2	5.08	10%
Alt. load	19.4-40.4	26	19	23.60	21.40	45			
		43	39			82			
H_3	16.6-41.0	9	18	14.15	12.85	27			
Effect of	41.0-58.0	13	15	14.69	13.31	28	2	10.76	1%
Max. load	65.0-80.0	21	6	14.15	12.85	27			
		43	39			82			

TABLE IX

EQUIVALENT K_T DURING PERIOD OF CRACK PROPAGATION

Spec. no	Load range	f_a	$r \times 10^6$	$Ne = \frac{1}{r}$	fa'	K_T
31/32	24 ± 13.4	8,000	1,300	77,000	7,500	3.6
71/72	6.0 ± 10.6	4,750	9.4	10.65×10^6	3,750	2.8
90	6.0 ± 10.6	4,750	15.6	6.42×10^6	4,100	2.9

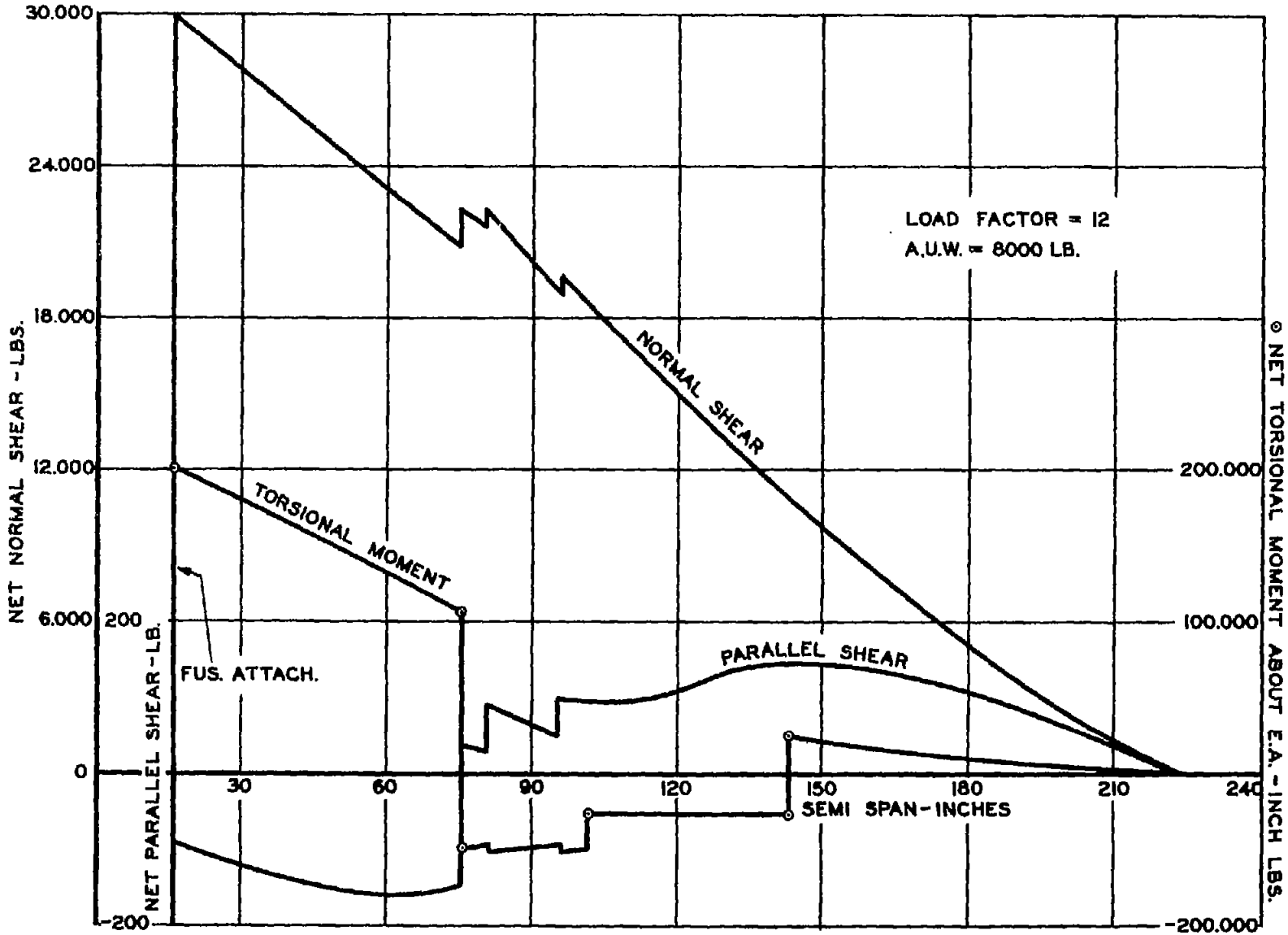

Figure 1.- Design shear and torsion diagram for load factor = 12.

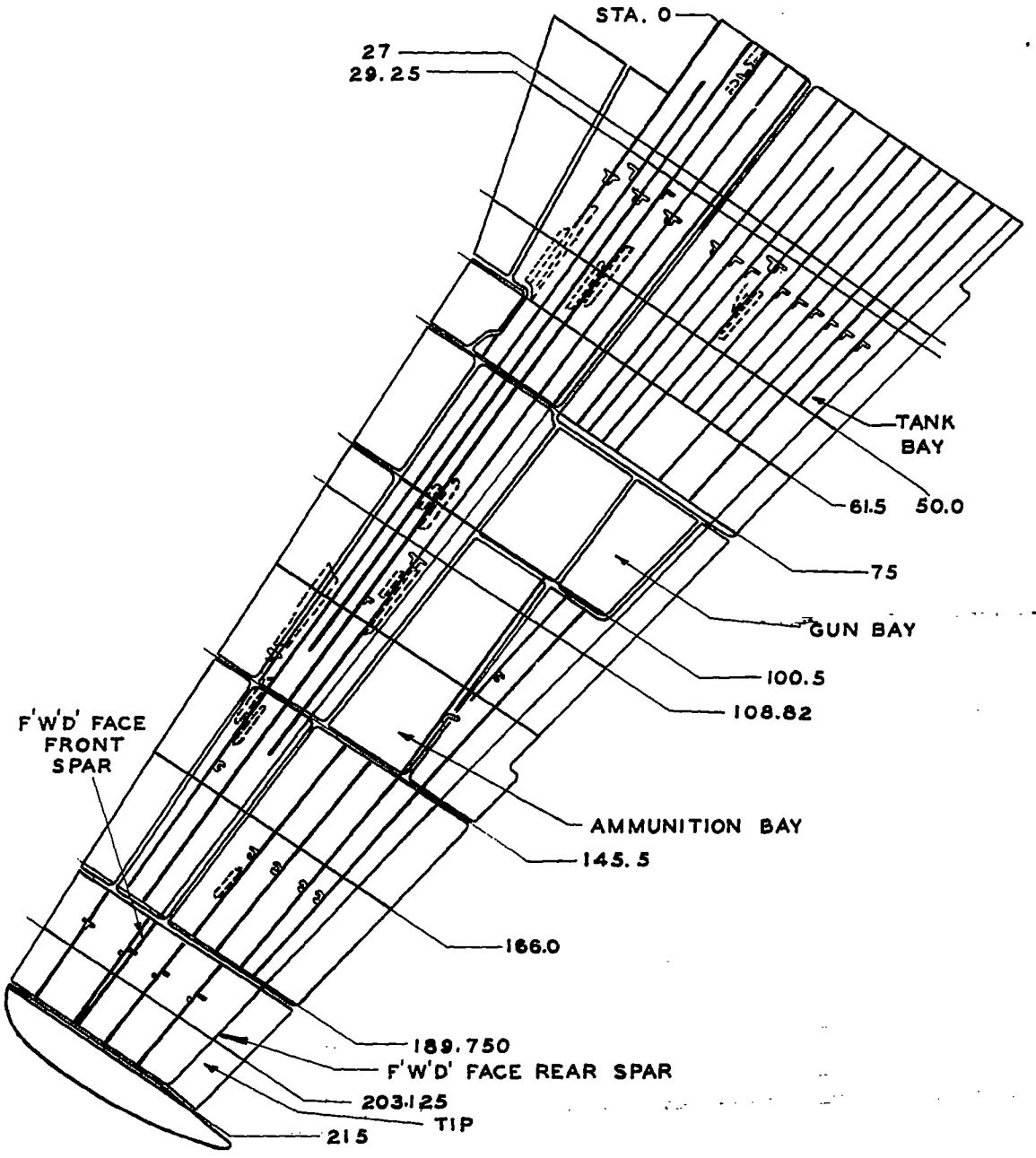

Figure 2.- P-51D wing stringer arrangement - upper surface.

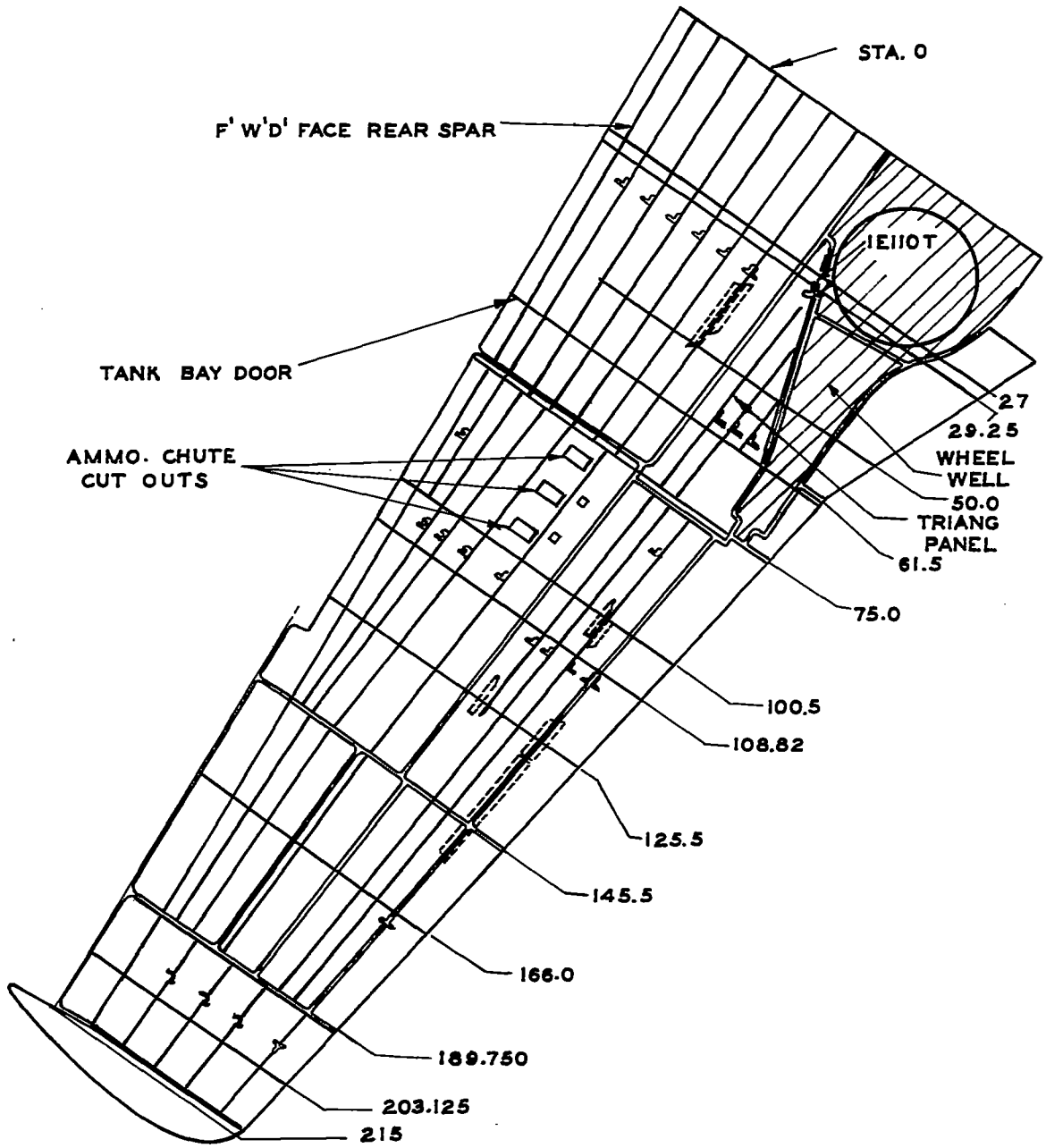

Figure 3.- P-51D wing stringer arrangement - lower surface.

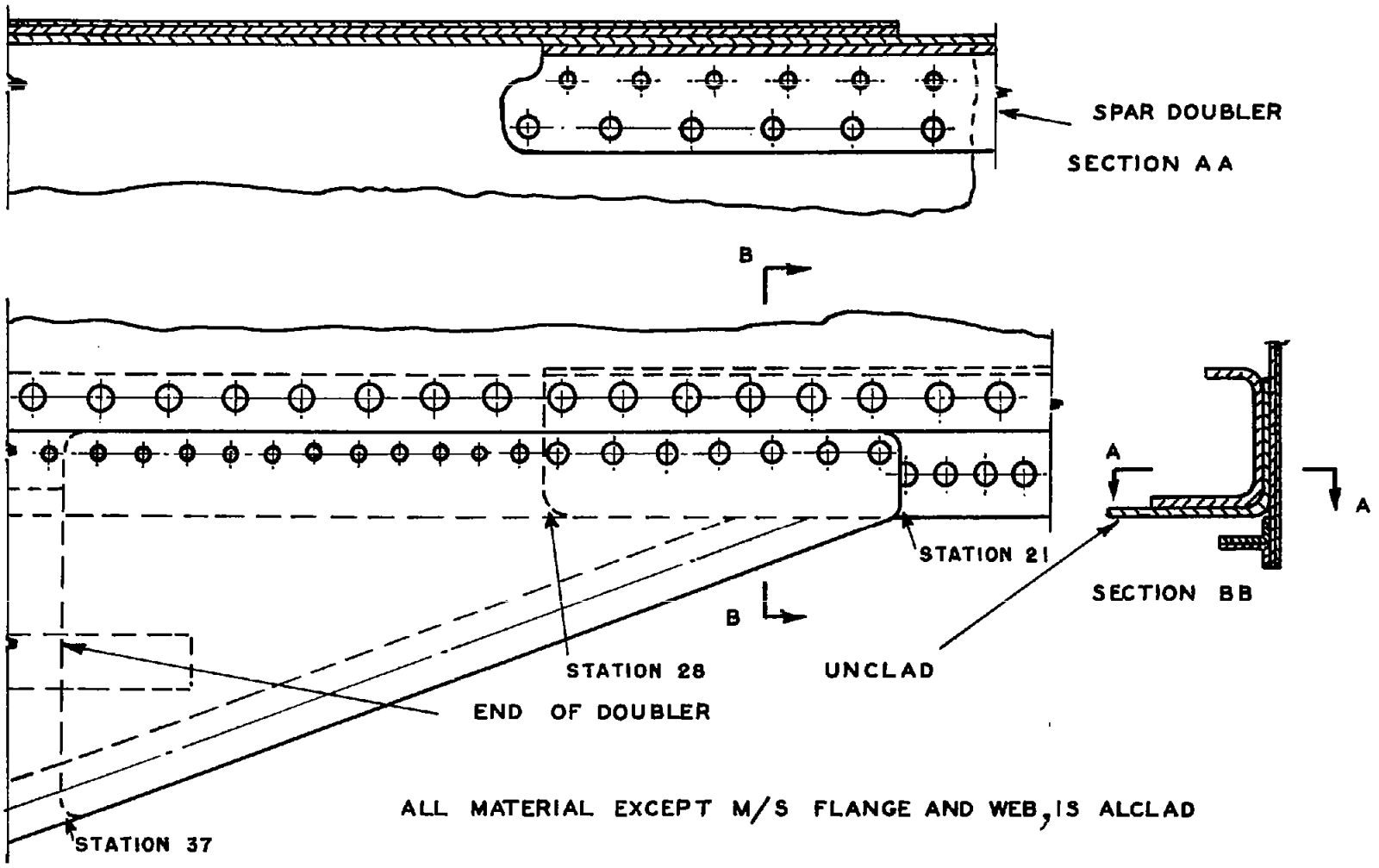

Figure 4.- Detail of main spar tension flange station 18 to station 38.

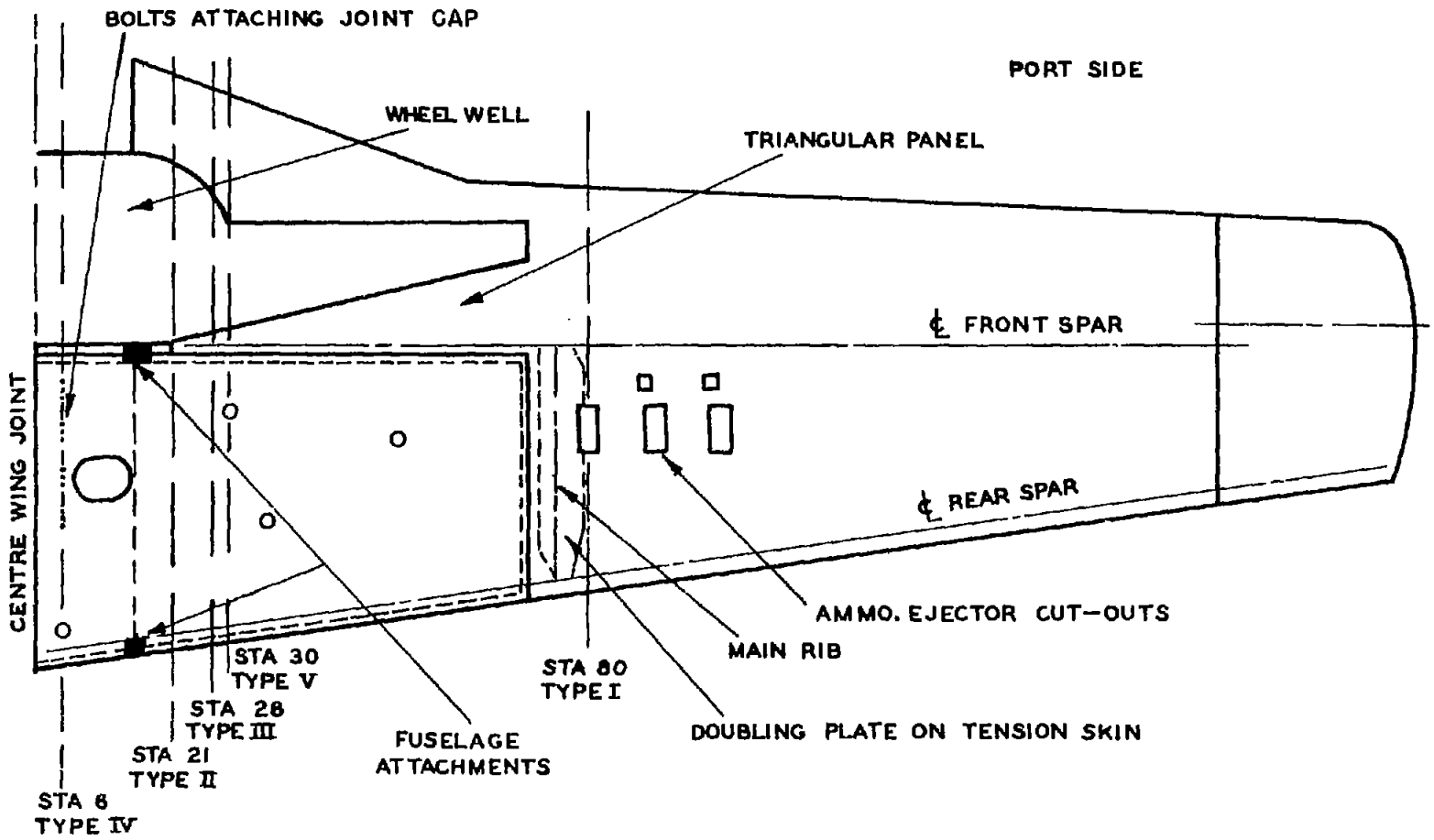

Figure 5.- View of wing lower surface showing position of major failures.

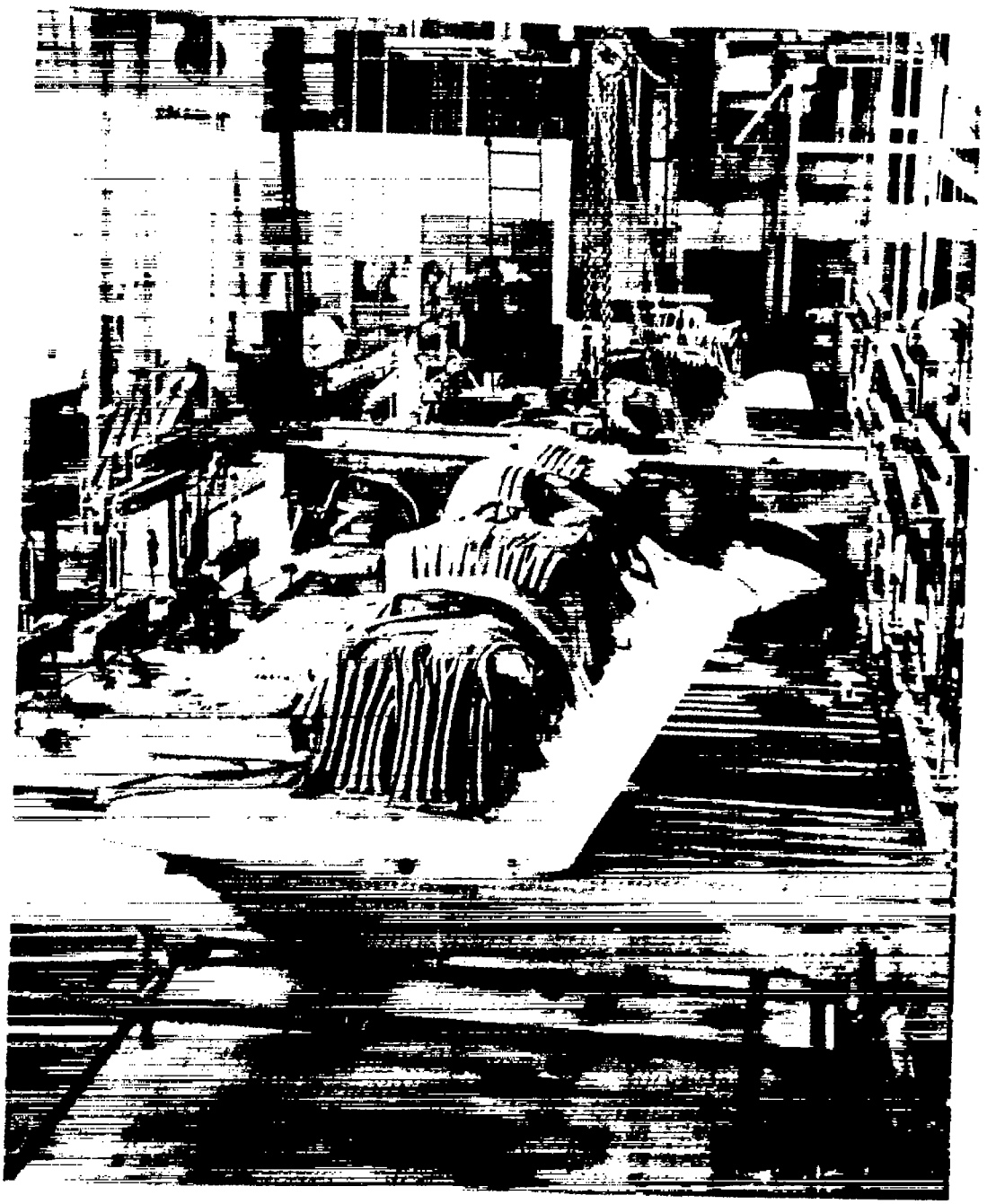

Figure 6.- Hydraulic loading rig with superimposed dead weight loading.

Figure 7.- Centre section support in hydraulic rig for superimposed dead weight loading.

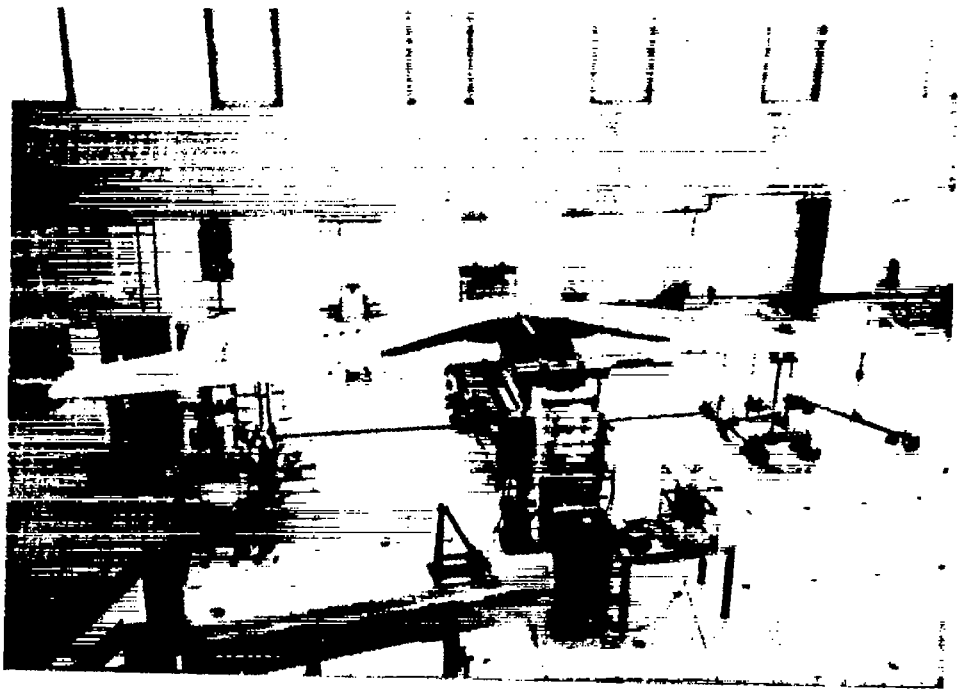

Figure 8.- General view of vibration loading rig.

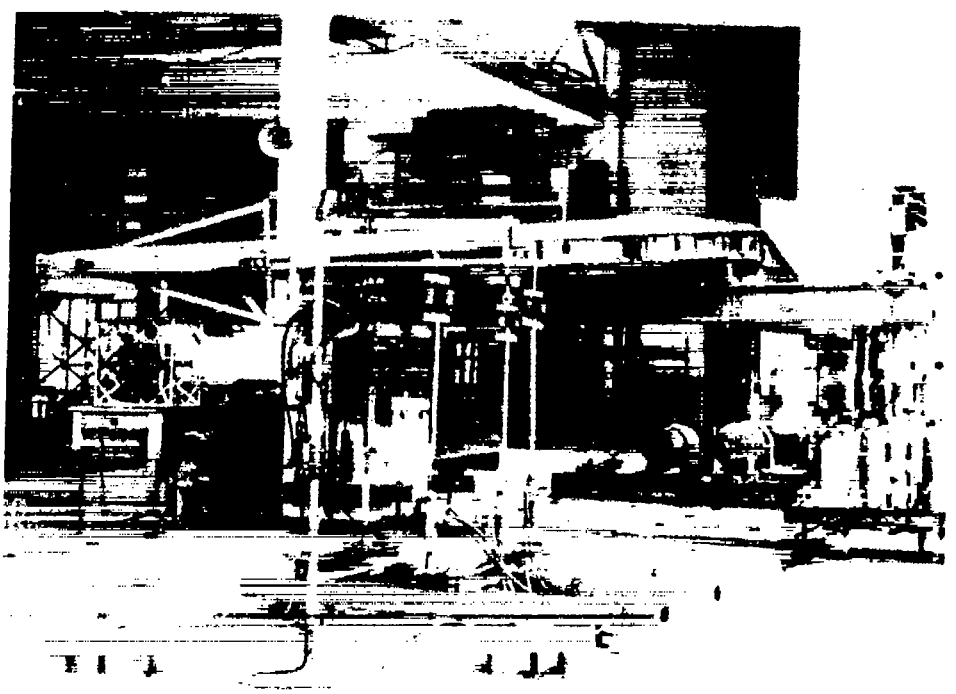

Figure 9.- Side view of vibration loading rig showing deflection indicator in foreground.

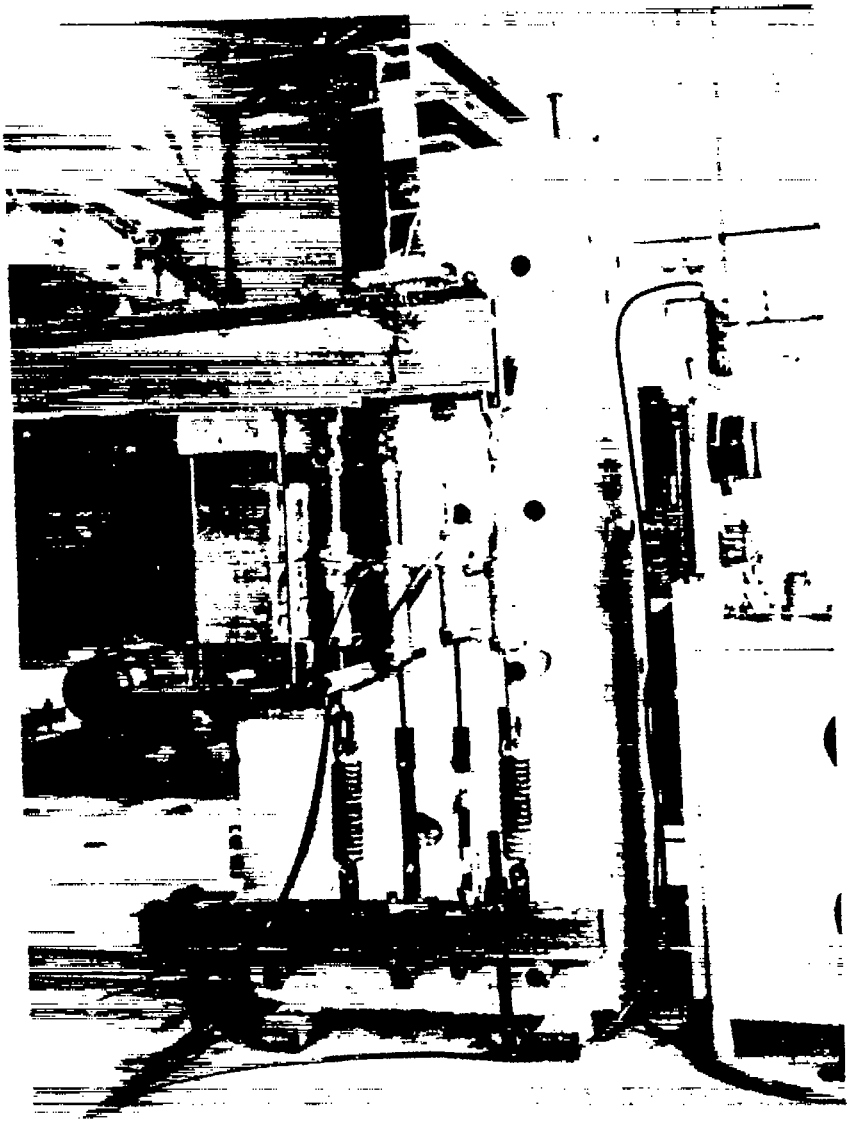

Figure 10.- Vibration loading rig rear support assembly.

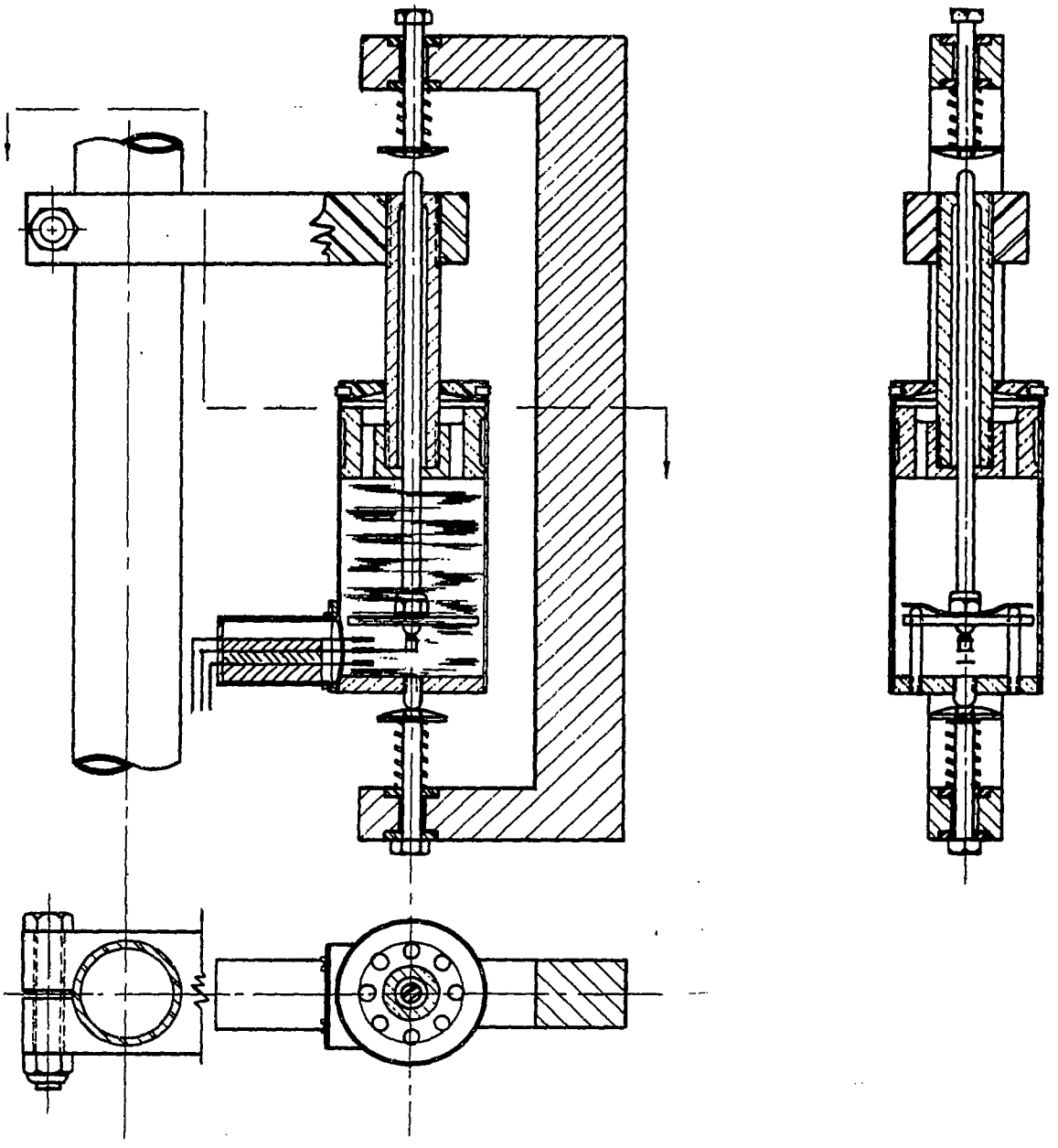

Figure 11.- Deflection indicator for vibration loading rig.

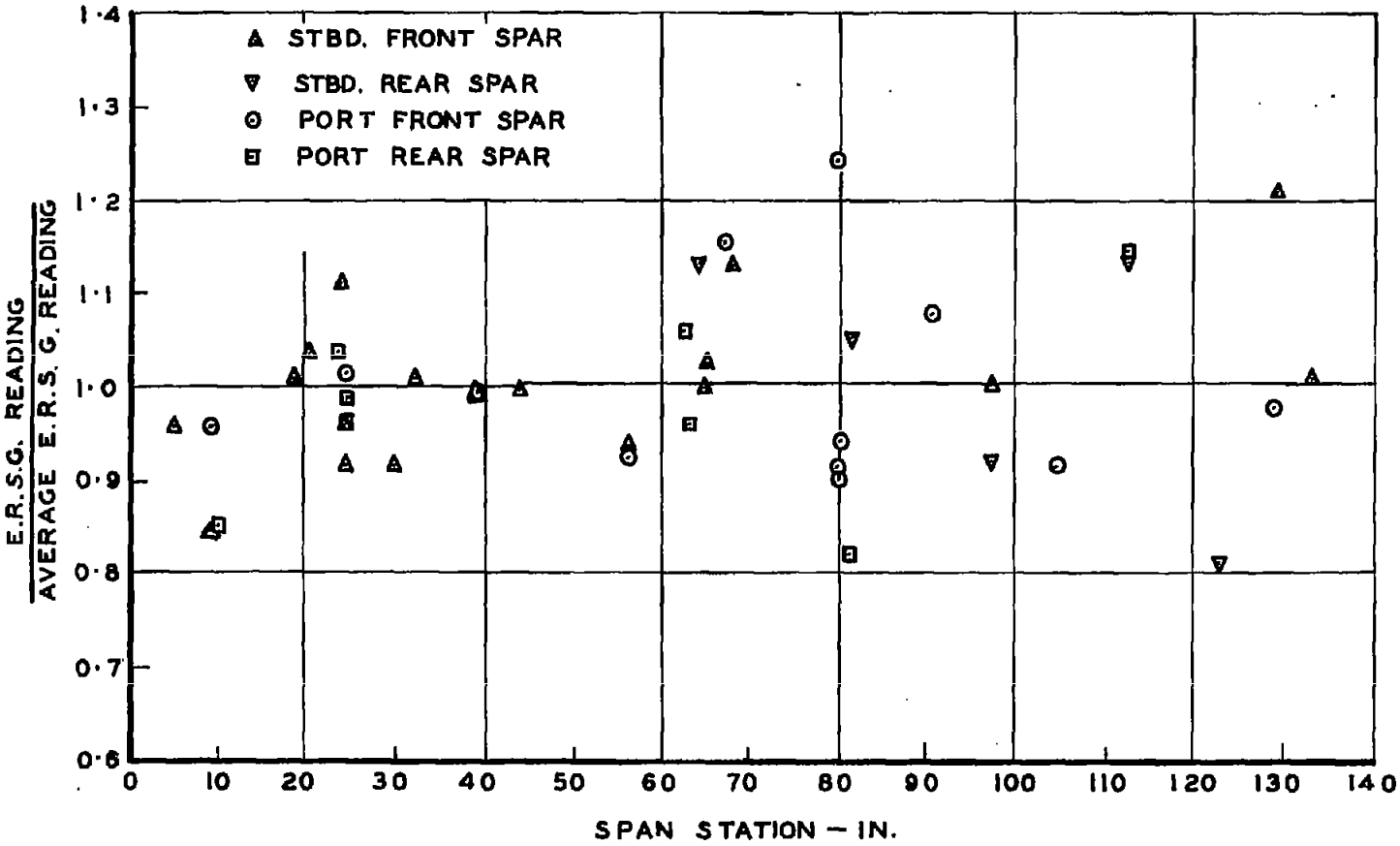

Figure 12.- Spanwise strain distribution from E.R.S.G. readings.

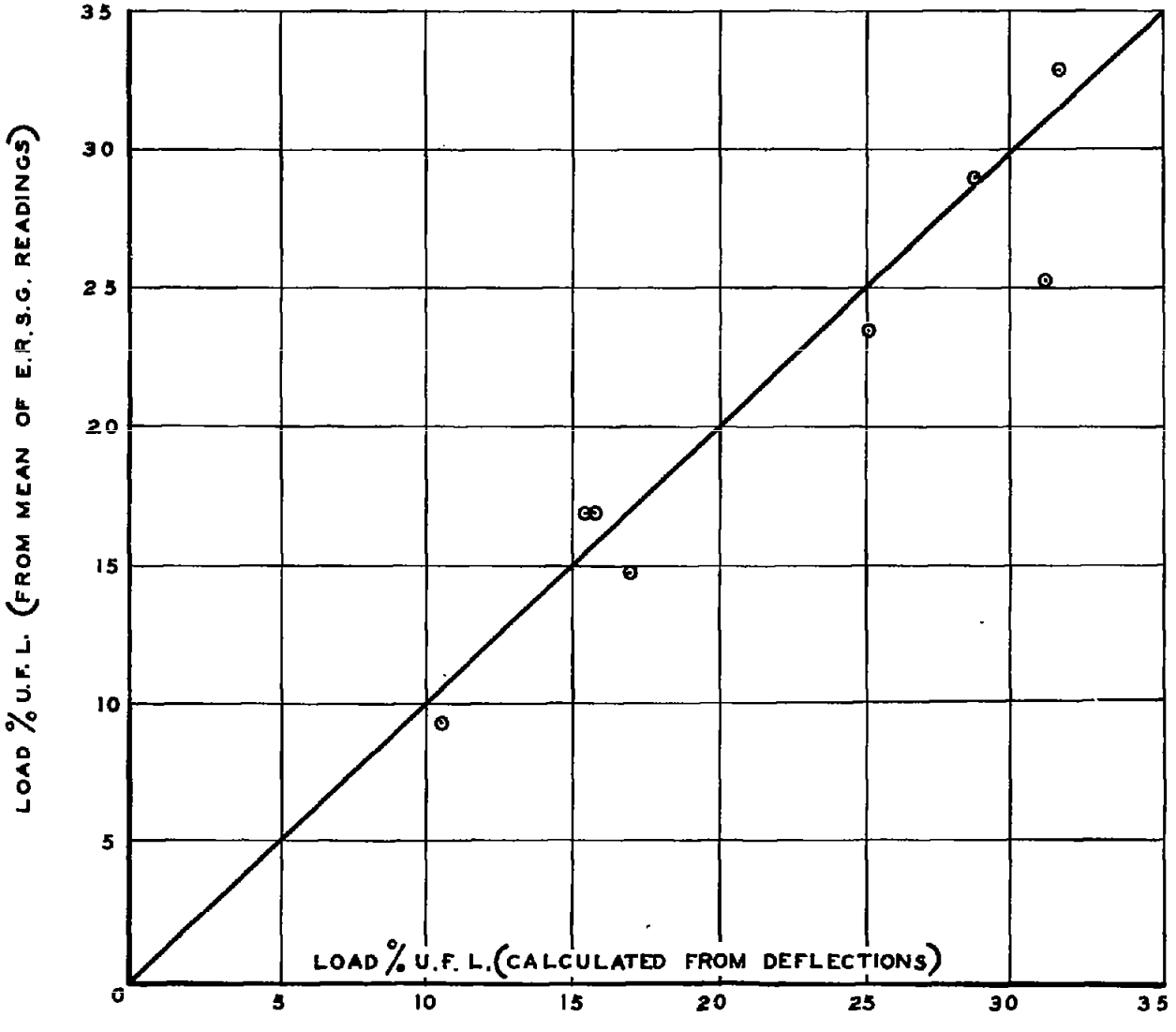

Figure 13.- Graph of strain gauge reading versus load.

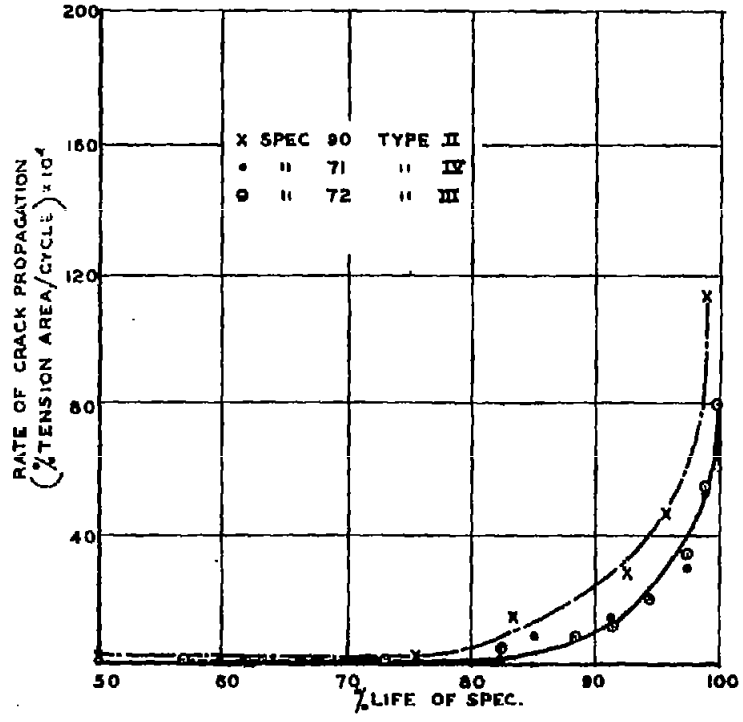

Figure 14.- Crack propagation rate.

Failure types II, III, IV.

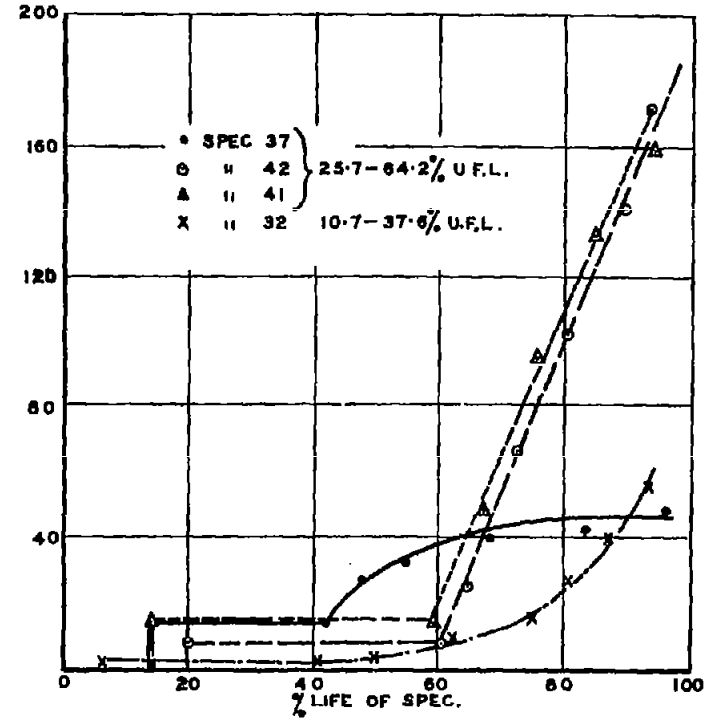

Figure 15.- Crack propagation rate.

Failure type I.

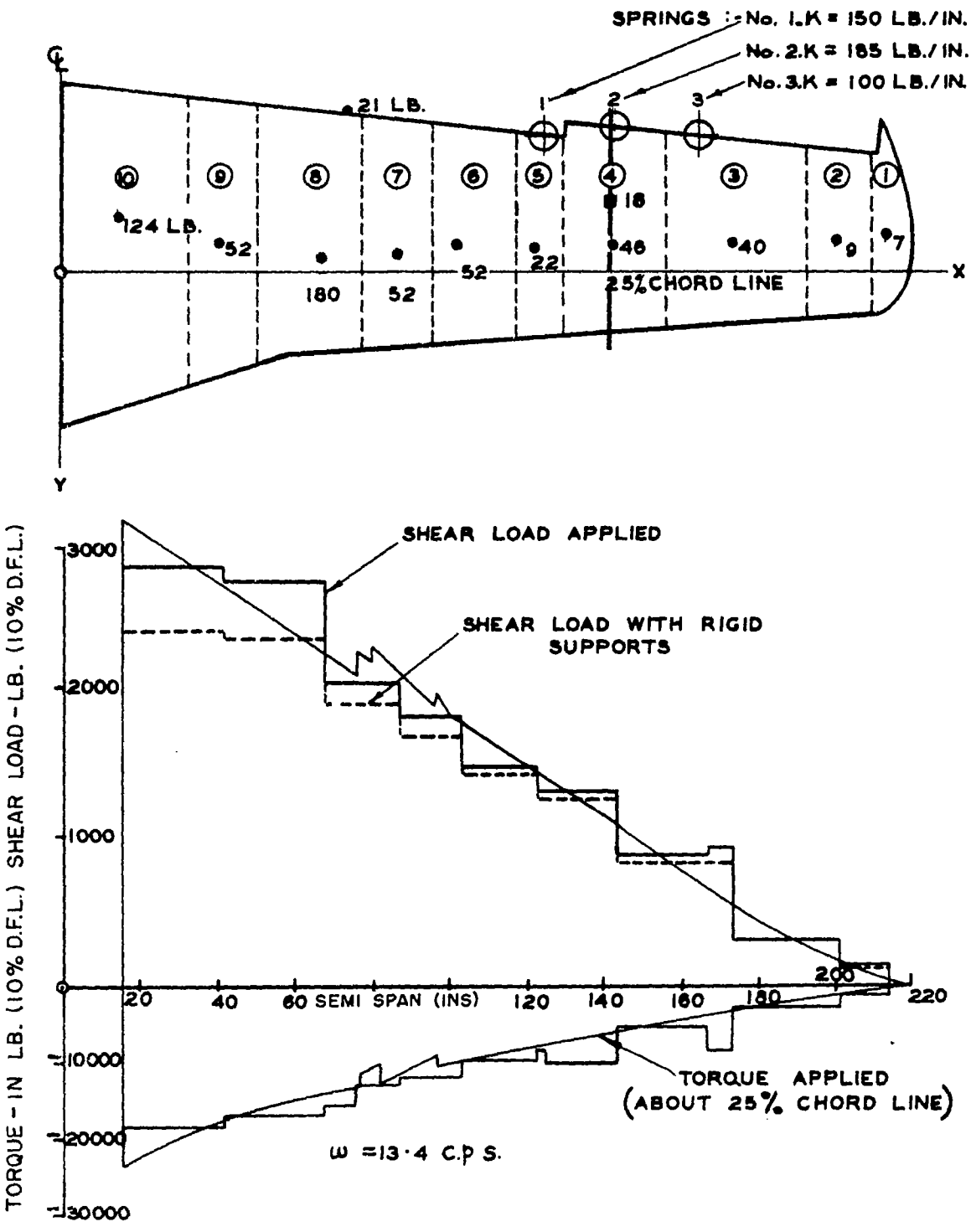

Figure 16.- Shear and torsion diagrams - vibration loading rig.

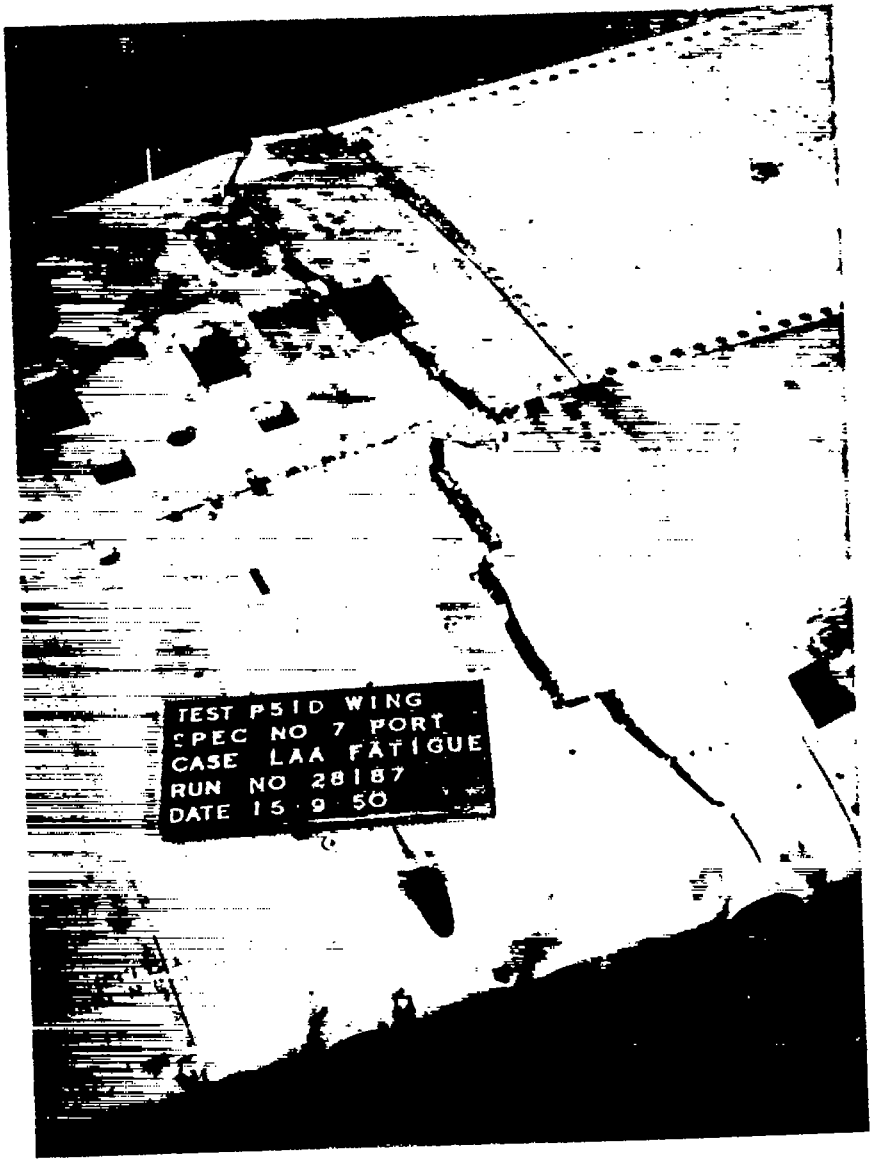

Figure 17.- Failure at station 80 - type I. Outer surface.

Figure 18.- Failure at station 80 - type I. Inner surface.

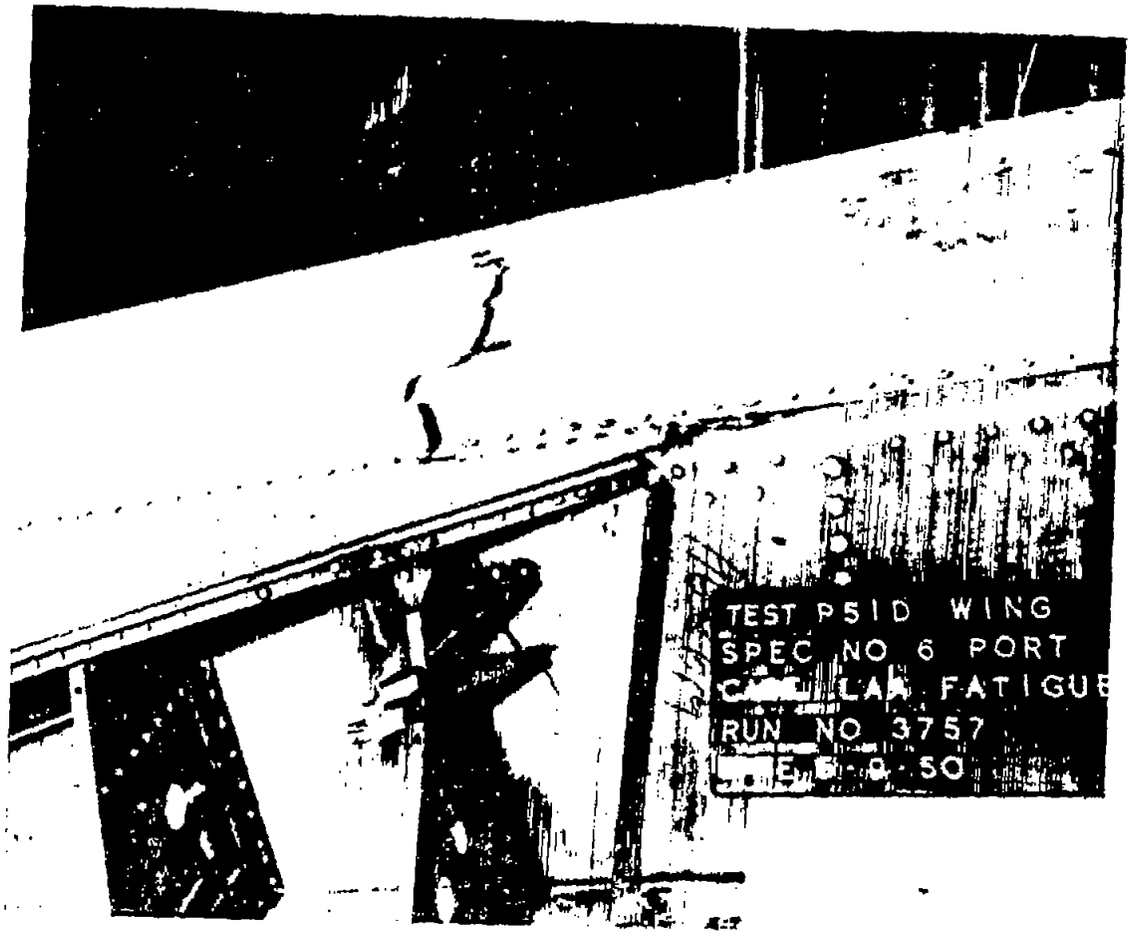

Figure 19.- Failure at station 28 - type III. (Similar failures occur at station 21 - type II, and at station 30 - type V.)

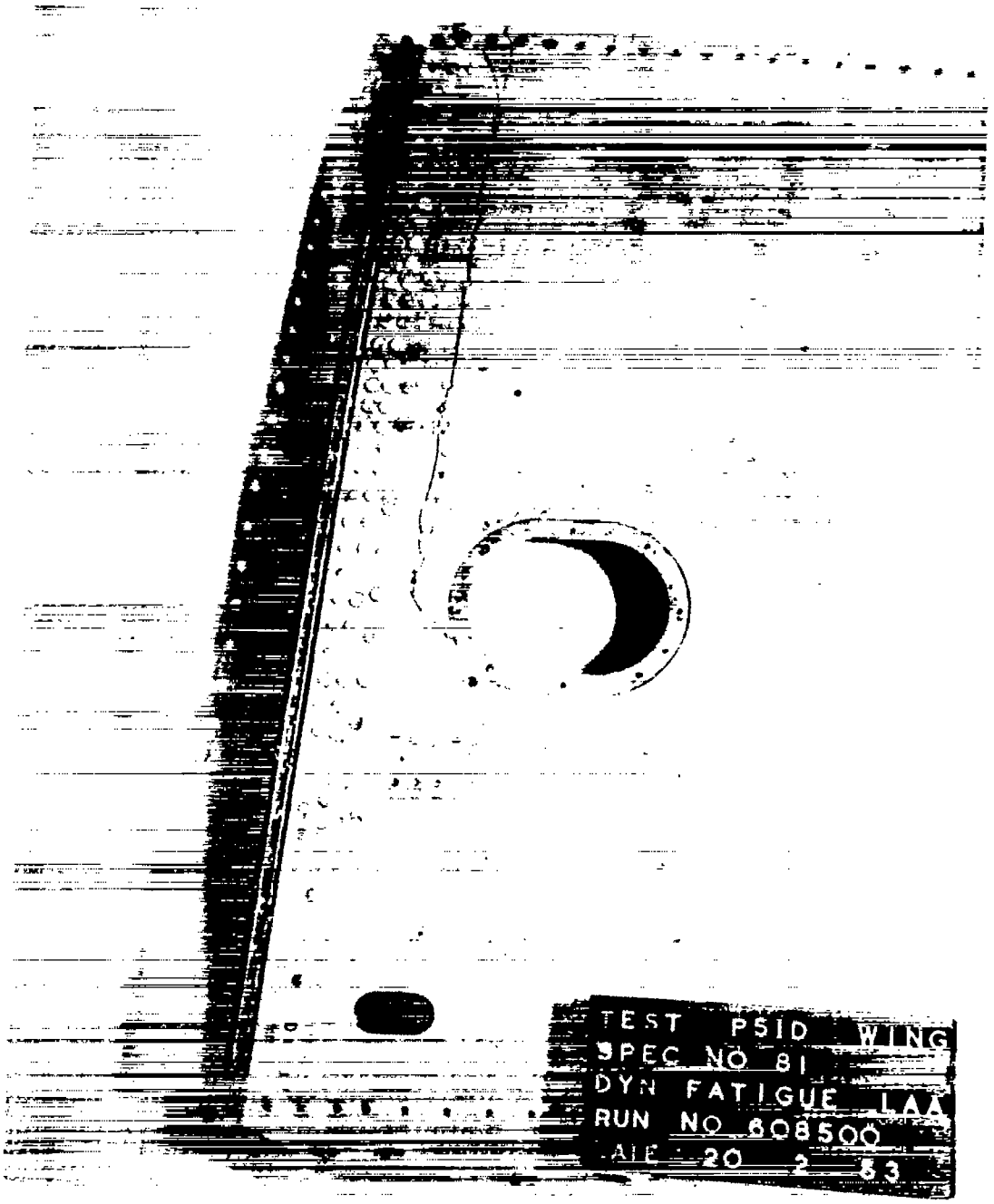

Figure 20.- Failure at station $\bar{6}$ - type IV.

Figure 21.- Failure in compression skin at station 100. (Initiation of failure, type VI.)

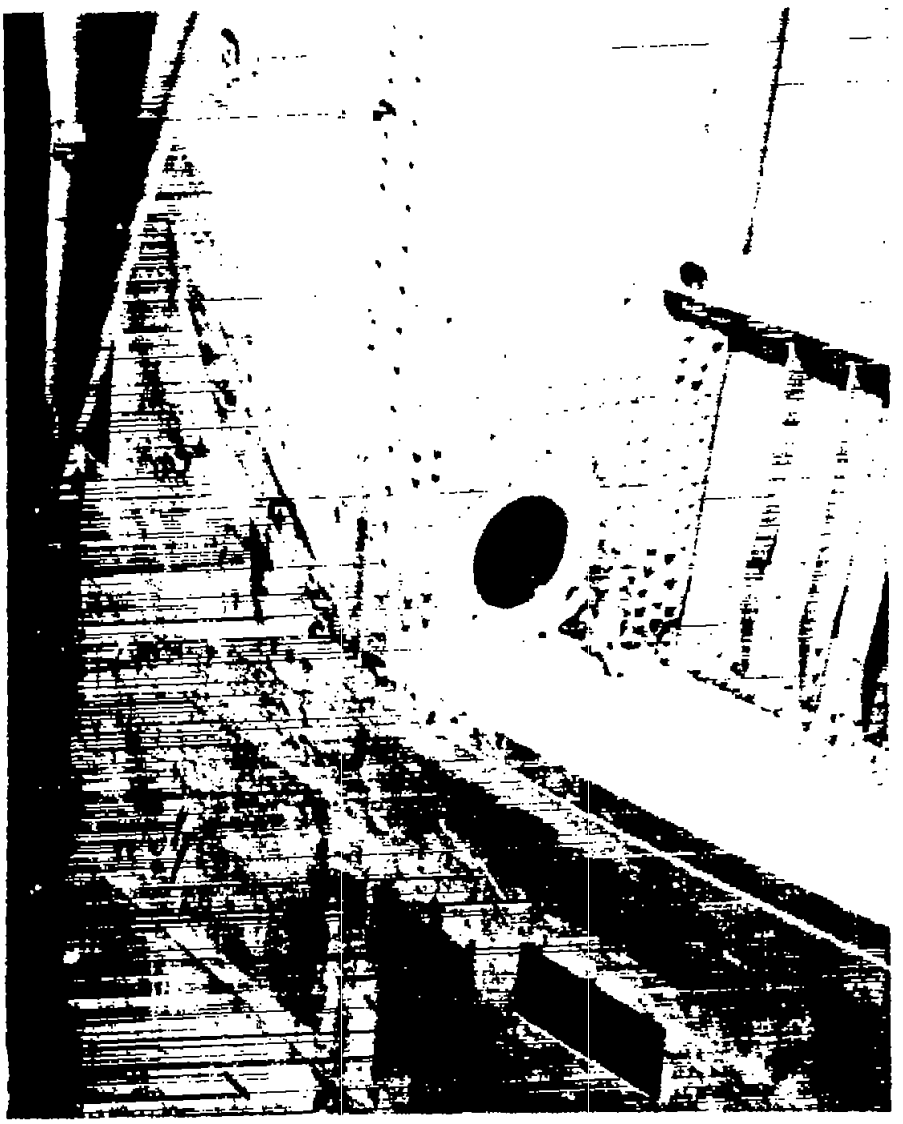

Figure 22.- Failures in tension skin at station 75. (Second stage of failure, type VI.)

Figure 23.- Failure in tension skin rearward at station 80. (Final stage of failure, type VI.)

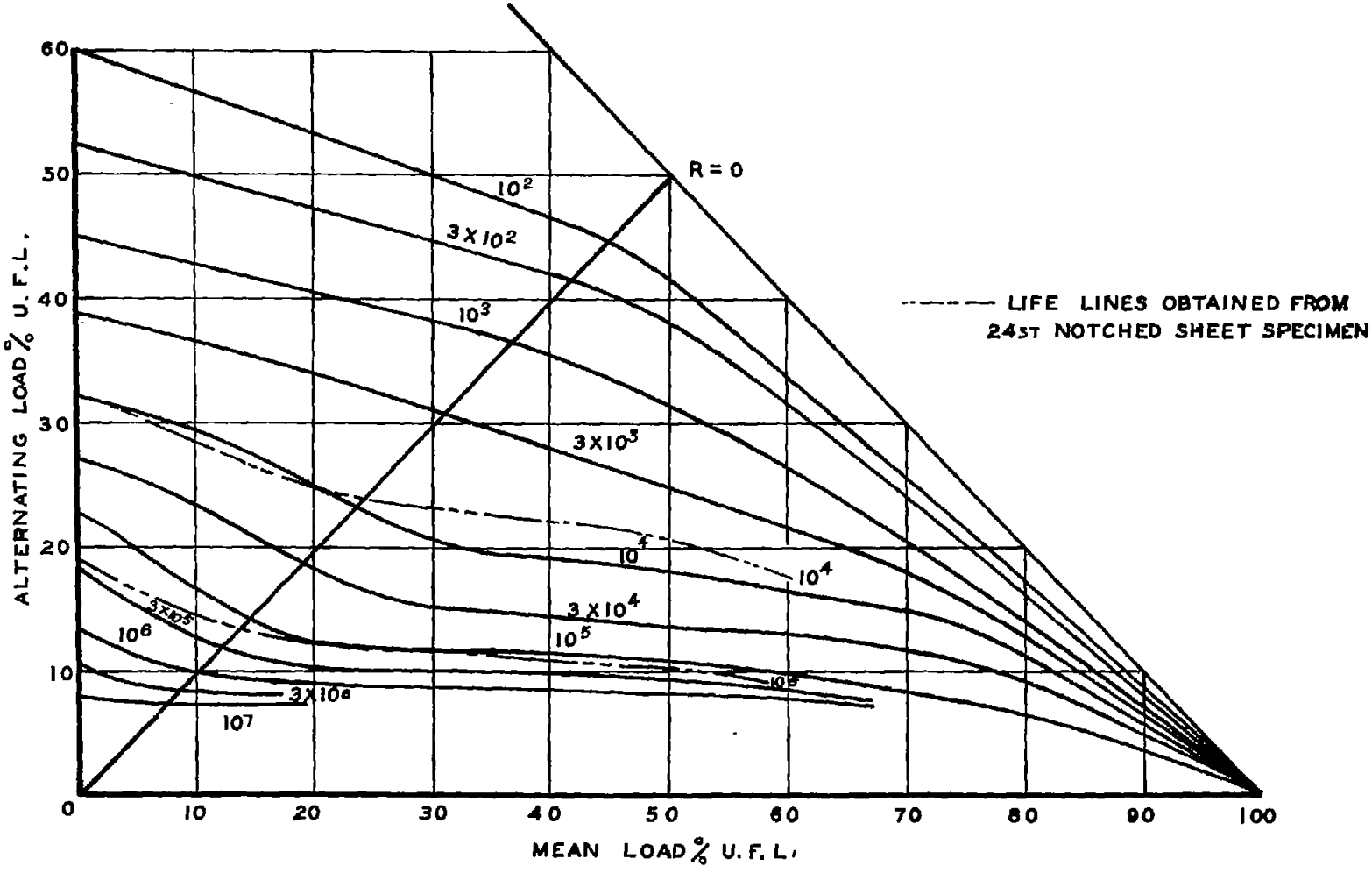

Figure 24.- Alternating load - mean load diagram.

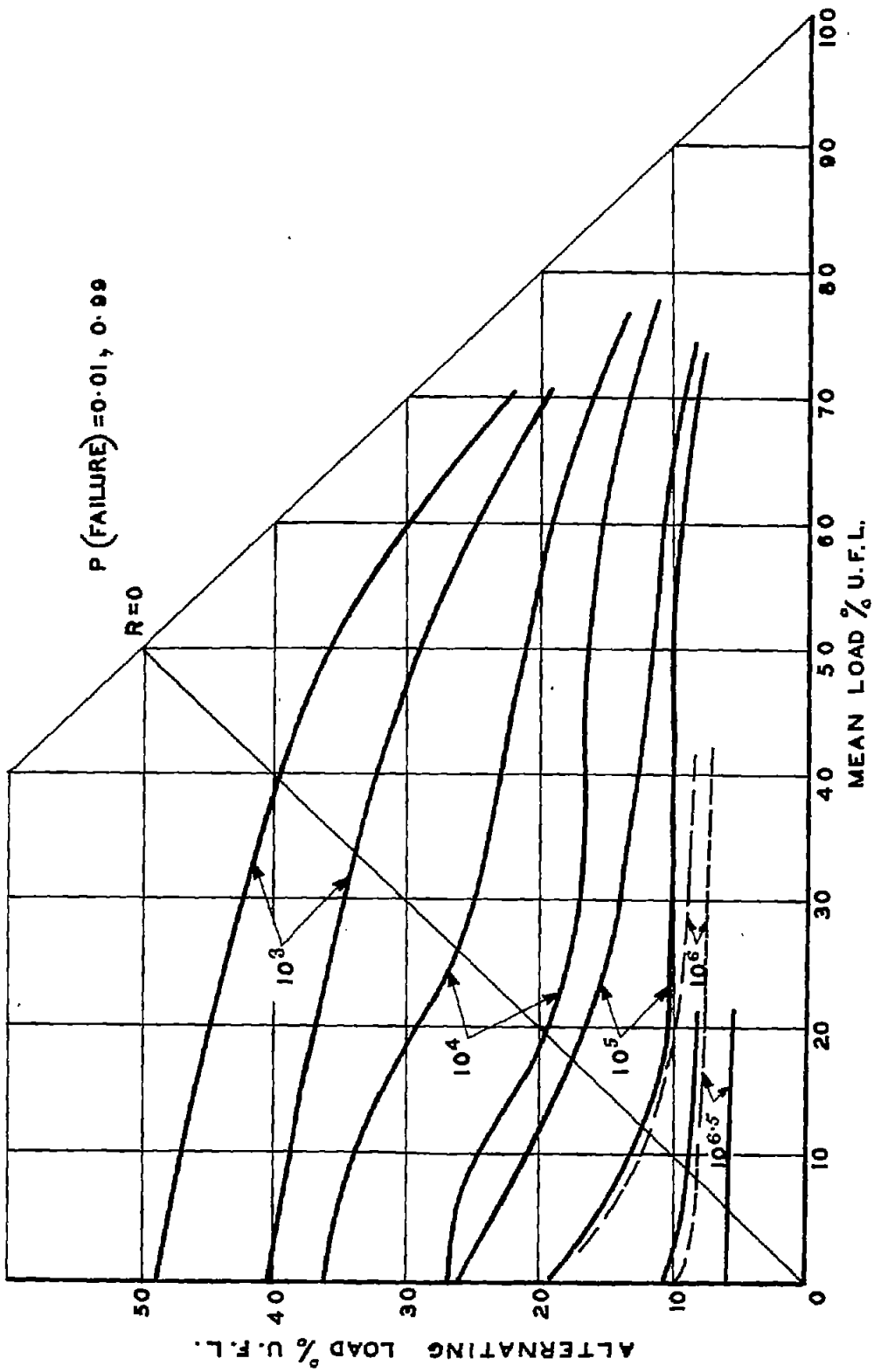

Figure 25.- A-M diagram scatter bands.

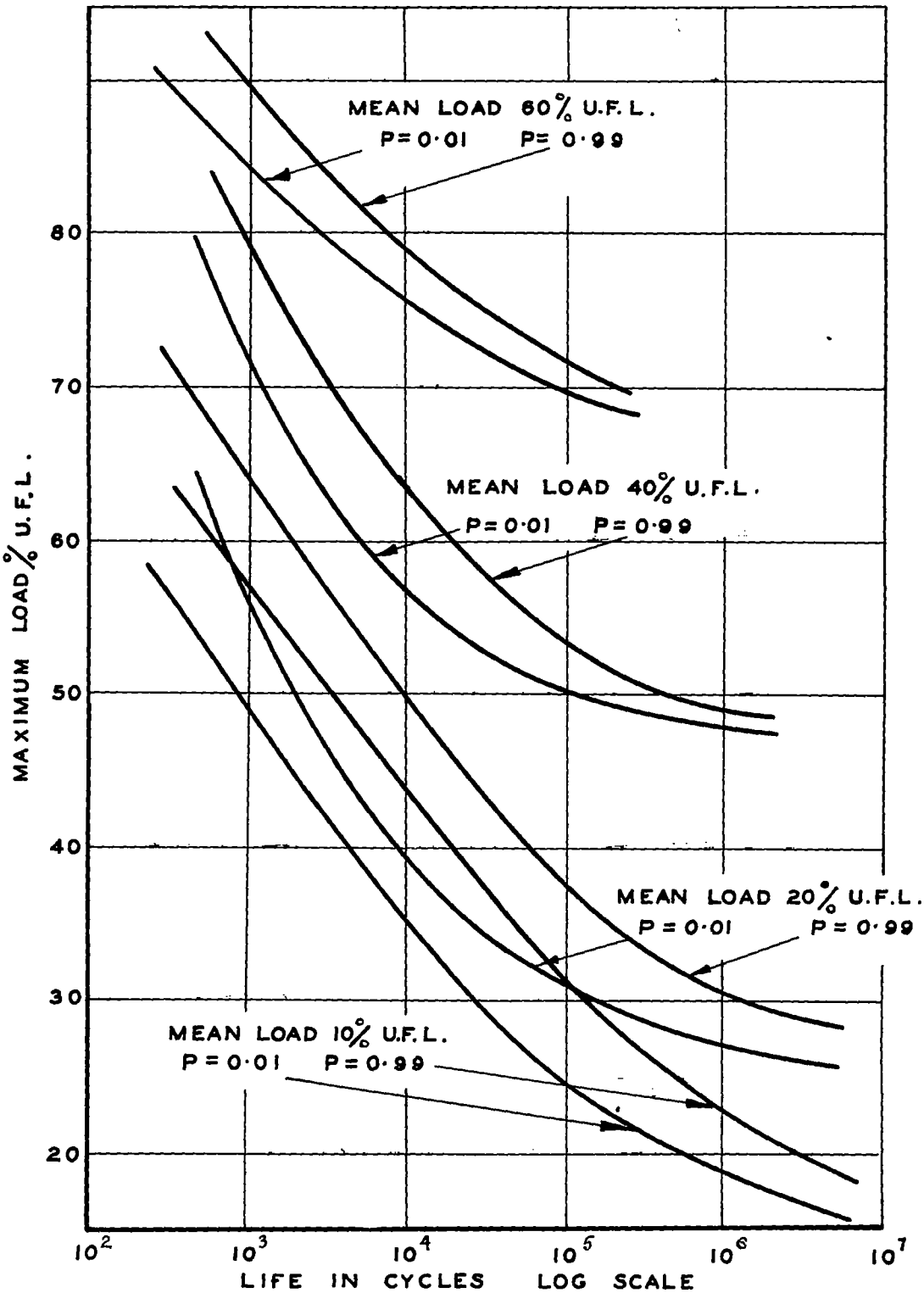

Figure 26.- S-N diagram scatter bands.

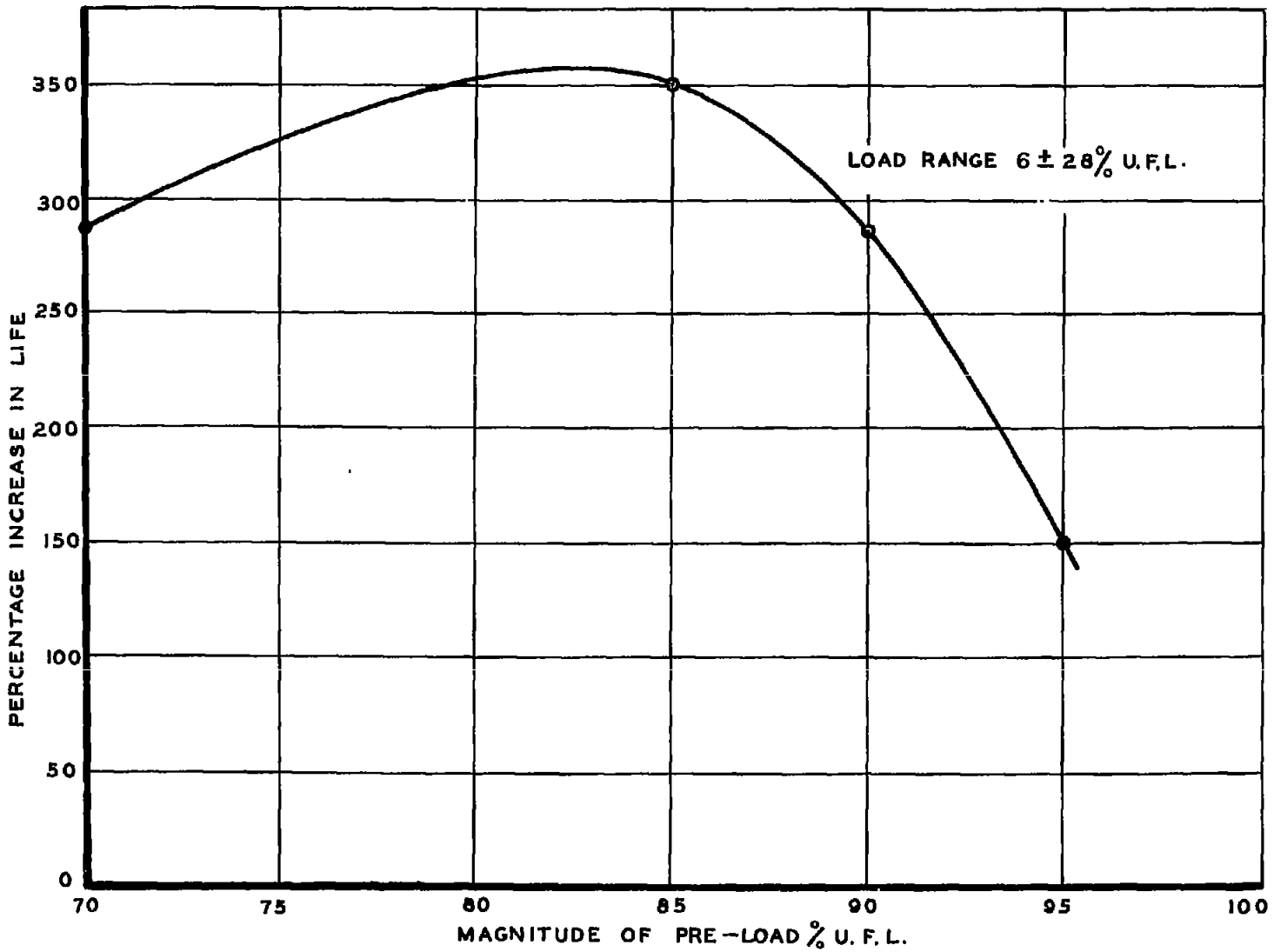

Figure 27.- Effect of pre-load on increase in life.

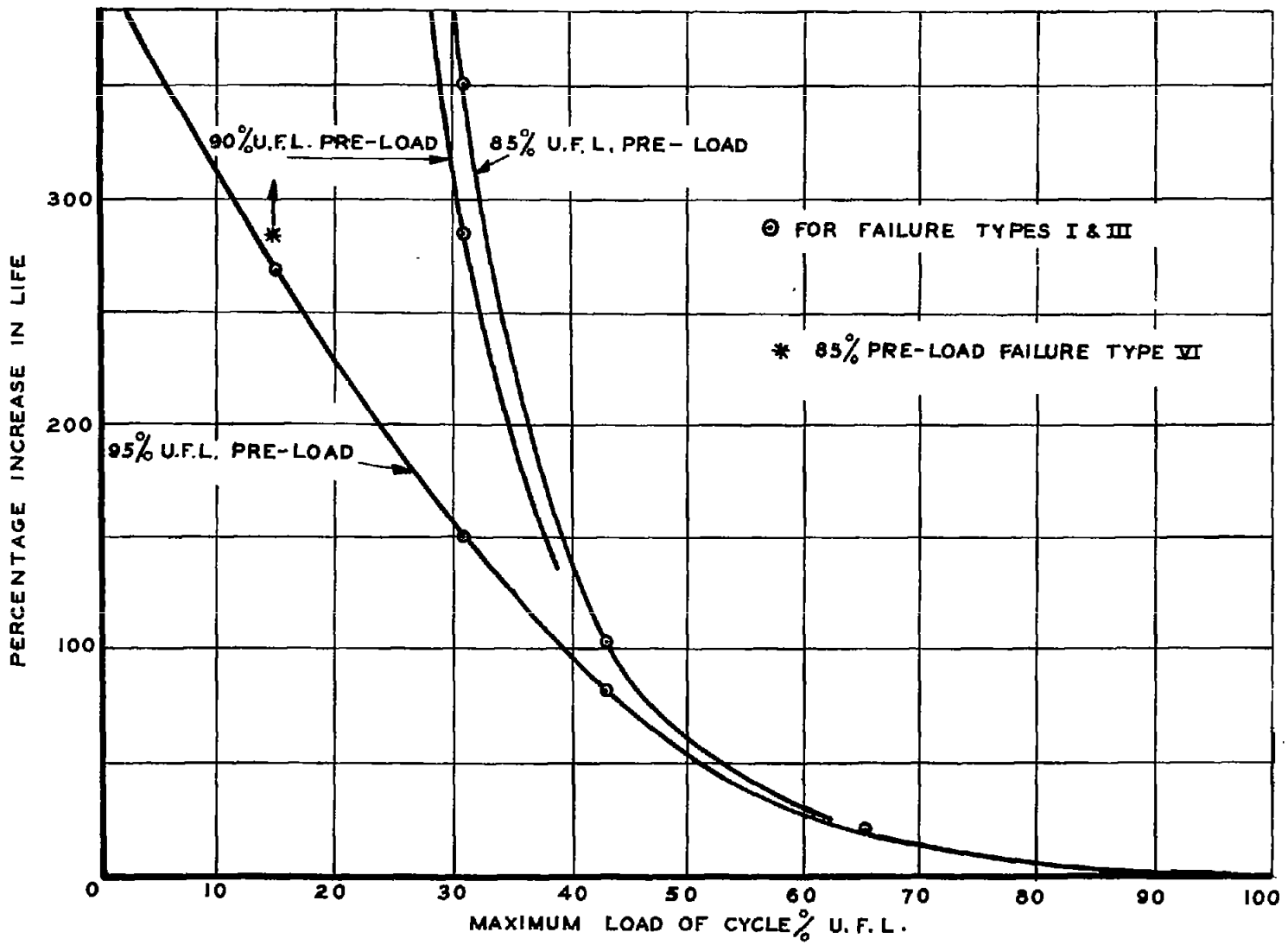

Figure 28.- Effect of pre-load and maximum load of cycle on increase in life.

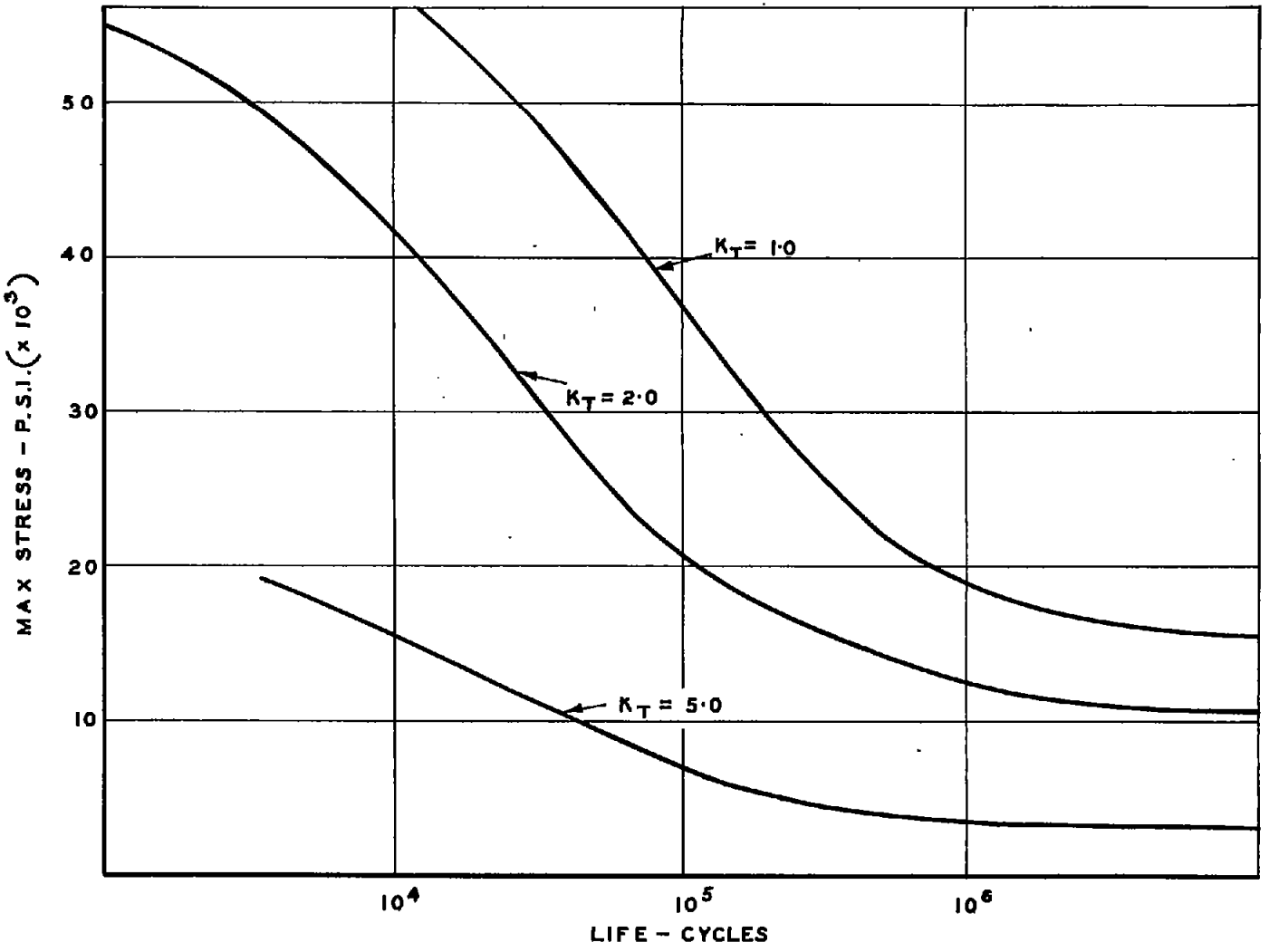

Figure 29.- SN curves (R = 0) for alclad 24ST at various K_T (refs. 8 and 9).

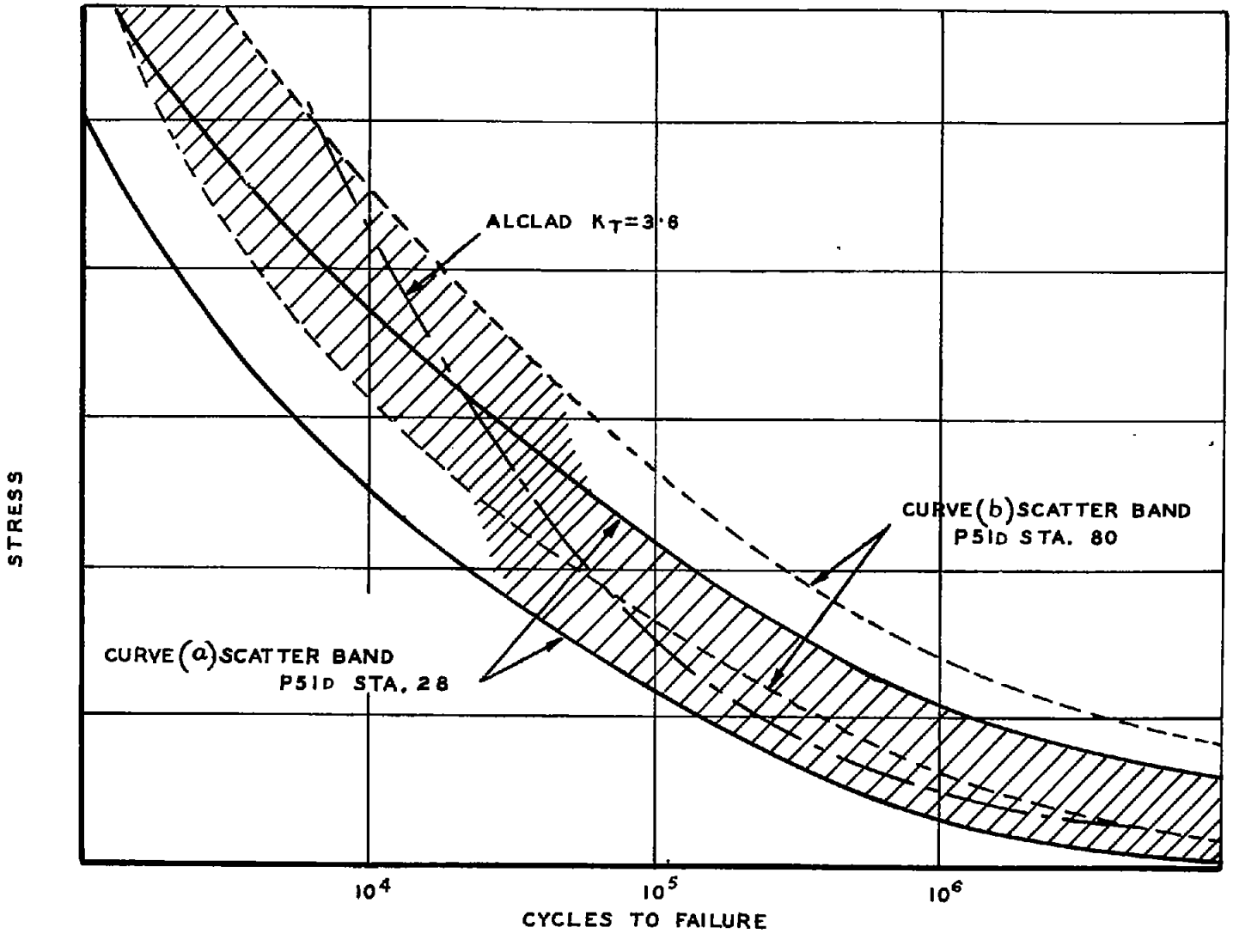

Figure 30.- Comparison of P51D mainplane with 24ST alclad. R = 0.

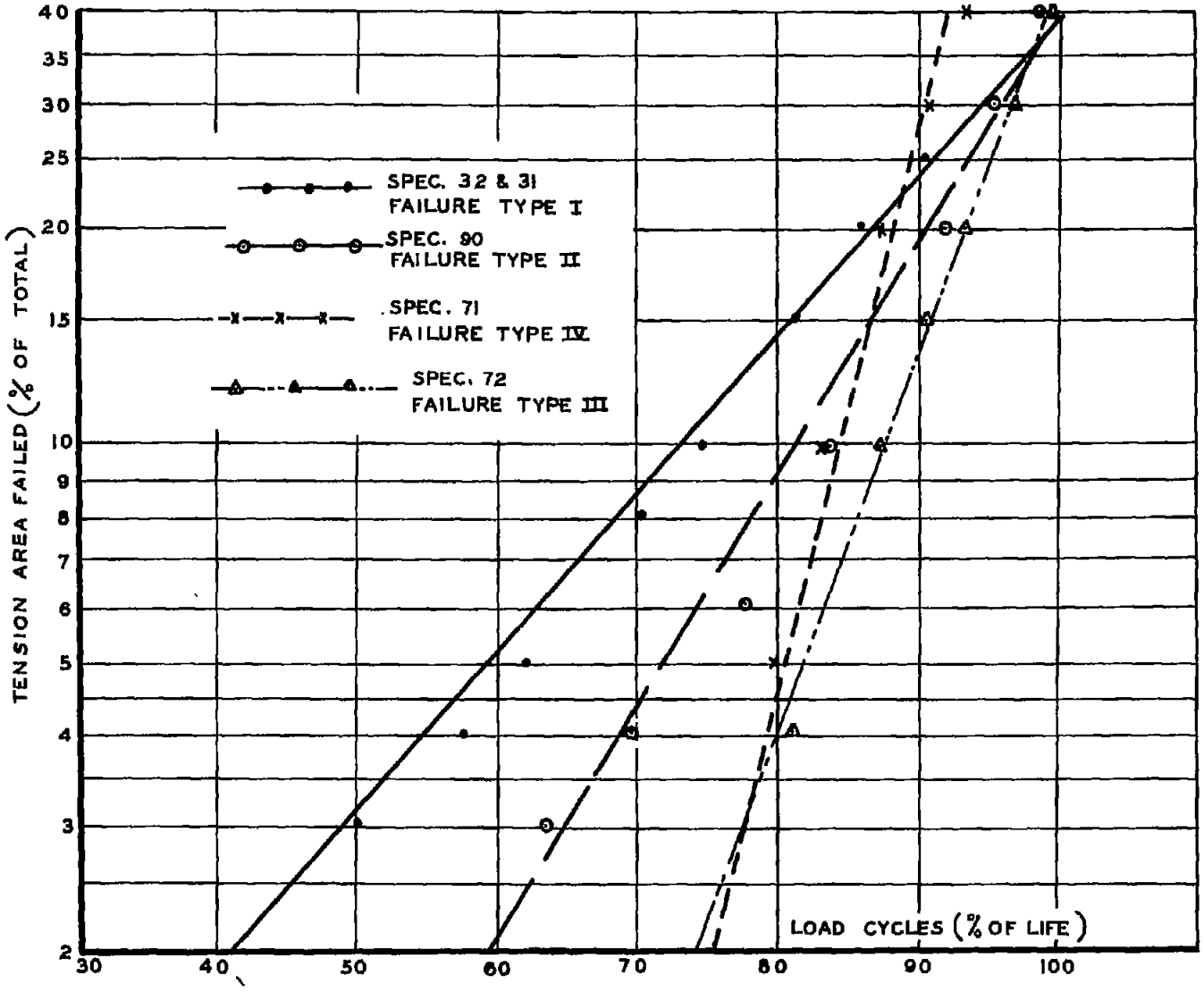

Figure 31.- Relation between damage and load cycles.

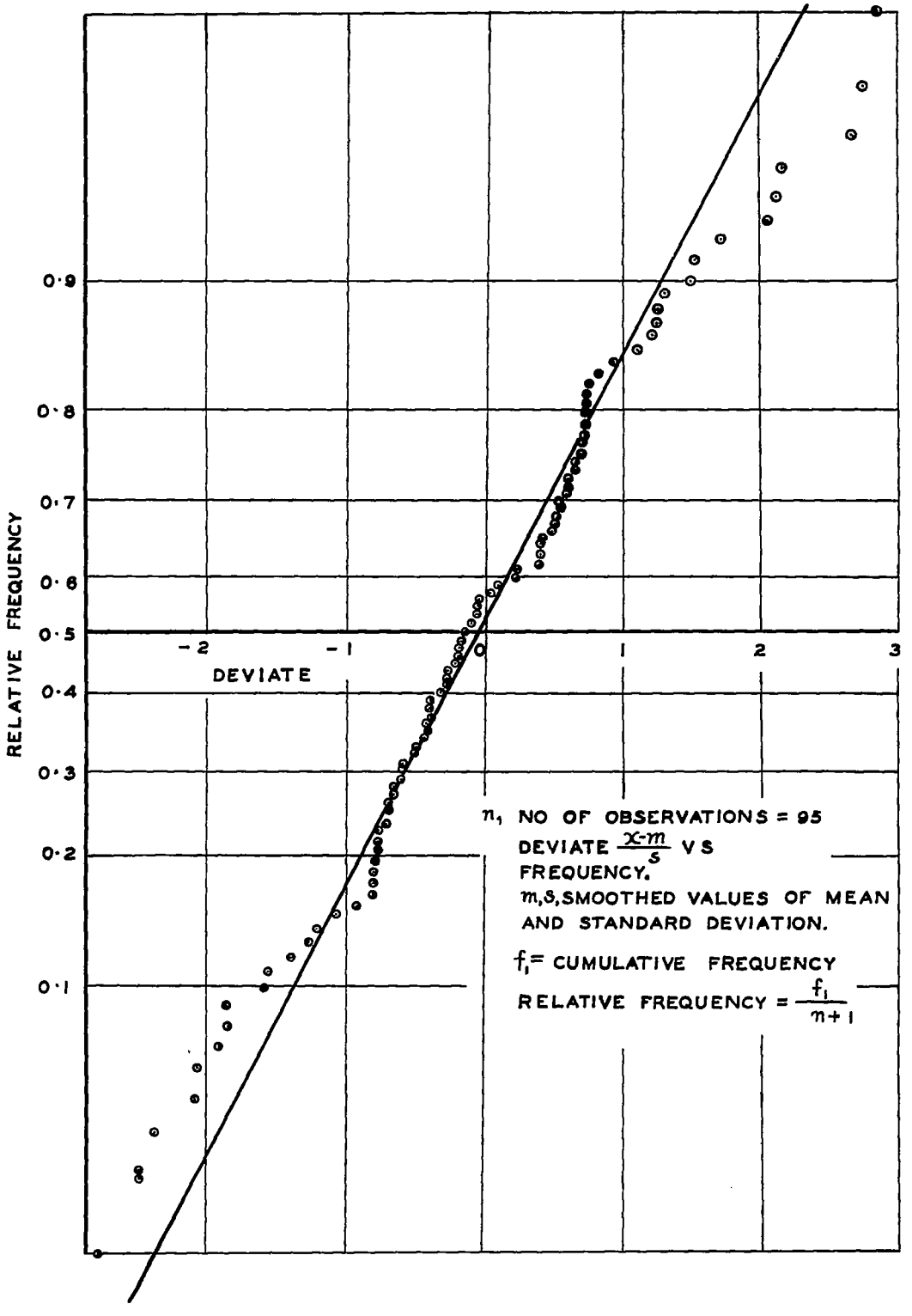

Figure 32.- Relative frequency for $\log_{10}N$.

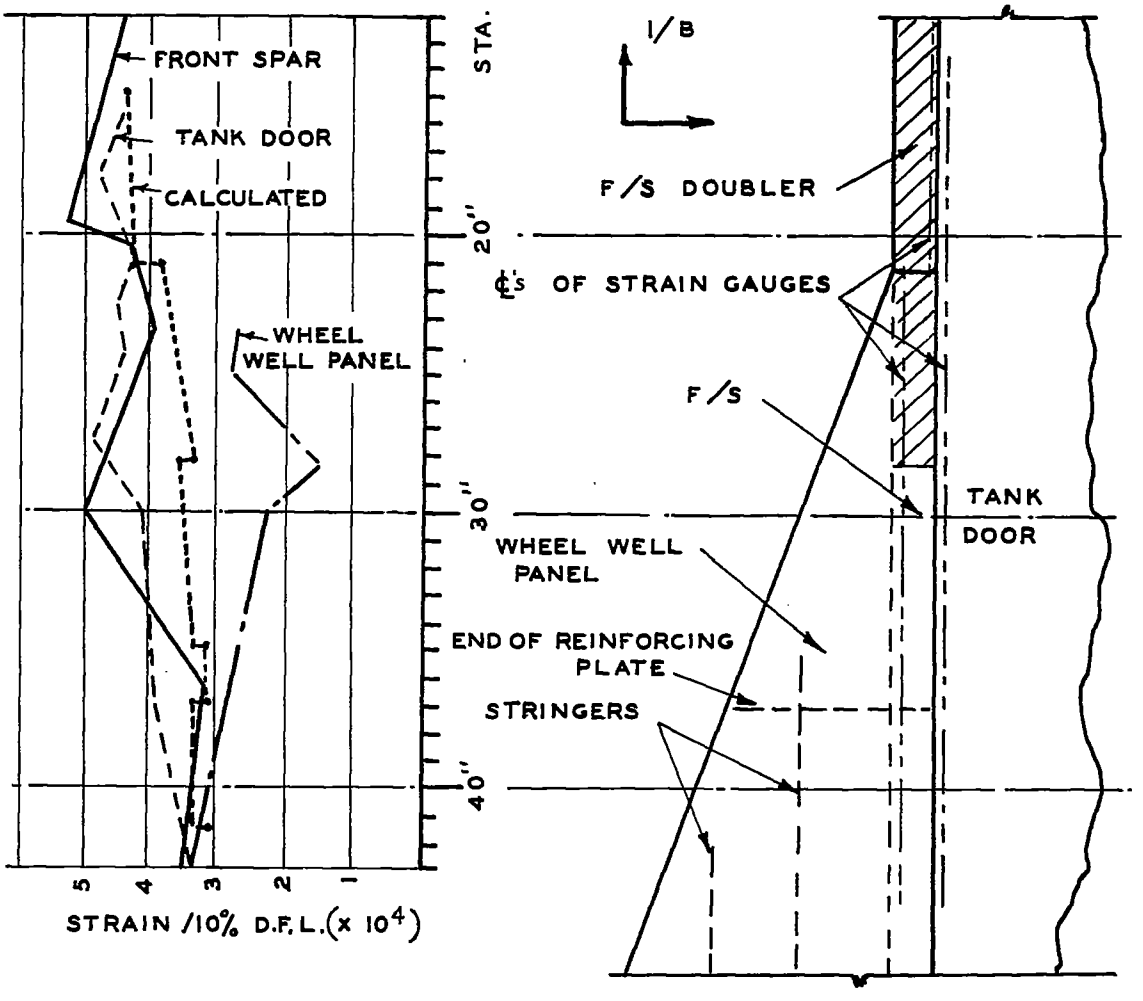

Figure 33.- Strain distribution in region of front spar in neighbourhood of station 28.

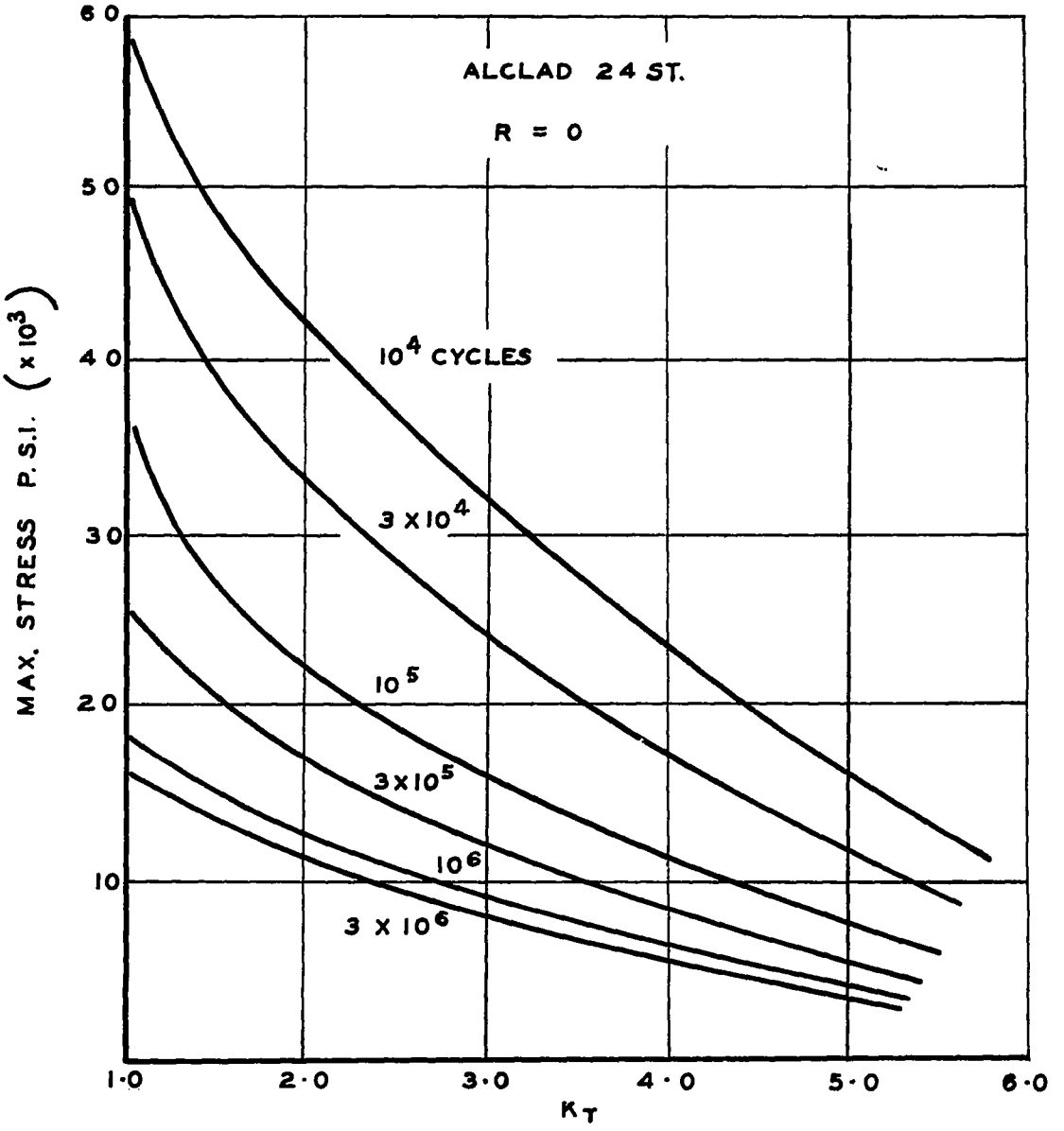

Figure 34.- Curves of stress versus S.C.F. for constant life.